Multi-functional ARF1 compartments serve as a hub for short-range cargo transfer to endosomes

Alexander Stockhammer[1,*], Petia Adarska[1,*], Vini Natalia[1], Anja Heuhsen[1], Antonia Klemt[1], Shelly Harel[1], Carmen Rodilla-Ramirez[1], Carissa Spalt[1], Ece Özsoy[1], Paula Leupold[1], Alica Grindel[1], Eleanor Fox[1], Joy Orezimena Mejedo[1], Dmytro Puchkov[2], Volker Haucke[1,2], Francesca Bottanelli[1,#]

[1]Freie Universität Berlin, Institute of Chemistry and Biochemistry, Thielallee 63, 14195 Berlin, Germany
[2]Leibniz Forschungsinstitut für Molekulare Pharmakologie (FMP), Robert-Rössle-Str. 10, 13125 Berlin, Germany

* These authors contributed equally

[#] Correspondence: francesca.bottanelli@fu-berlin.de

Abstract
Cellular membrane homeostasis is maintained via a tightly regulated membrane and cargo flow between organelles of the endocytic and secretory pathways. Adaptor protein complexes (APs), which are recruited to membranes by the small GTPase ARF1, facilitate cargo selection and incorporation into trafficking intermediates. According to the classical model, small vesicles would facilitate bi-directional long-range vesicular transport between the Golgi and endosomes. Here we revisit the intracellular organization of the vesicular sorting machinery using a combination of CRISPR-Cas9 gene editing, live-cell high temporal (fast-confocal) or spatial (stimulated emission depletion (STED)) microscopy as well as correlative light and electron microscopy. We characterize novel tubulo-vesicular ARF1 compartments that harbor clathrin and different APs, and coordinate Golgi export as well as endocytic recycling. Rather than long-range vesicle shuttling, we observe transient interactions of ARF1 compartments and recycling endosomes, with the sorting machinery localizing at the interface between the two membranes. Our findings suggest that endocytic and secretory cargo transfer from ARF1 compartments to endosomes may be mediated by a kiss-and-run mechanism rather than by fusion of transport vesicles.

Introduction

Eucaryotic cells compartmentalize biochemical reactions within membrane bound organelles. Material exchange occurs either via transport carriers that bud from a donor- and fuse with an acceptor-compartment or via direct contact between membranes. The Golgi apparatus and endosomal organelles are crucial for maintaining cellular membrane homeostasis as they coordinate the busiest trafficking highways at the intersection between exocytic and endocytic traffic. According to current models, communication between the Golgi and various endosomes is mediated by clathrin-coated vesicles[1,2]. Vesicle formation is orchestrated by a complex protein machinery, which ensures the specificity of cargo selection and guides trafficking intermediates to their correct destination within the cell. For this, key cargo adaptors such as the adaptor protein complex 1 (AP-1) are recruited to membranes by the ADP-ribosylation factor 1 (ARF1)[2-4], where they can recruit cargo and coat proteins such as clathrin to drive membrane curvature and vesicle formation[1,5].

When imaged as fusion proteins or with antibodies, clathrin and adaptors define punctate structures throughout the cytoplasm of the cell, supporting a vesicular model for cargo exchange between organelles[6-9]. In contrast to shuttling vesicles and full-collapse fusion events, intracellular organelle communication through a kiss-and-run mechanism was proposed[10,11]. First described in neurons[12], kiss-and-run events enable organelles to exchange material through transient pore formation, yet the involved compartments retain their identity, and putative diffusion barriers would avoid lipid and content mixing. Material exchange between organelles in a kiss-and-run fashion would require direct organelle interaction and the presence of a tubular endosomal network where endosomal compartments could closely interact[13]. Various secretory and endocytic recycling cargoes were found to traffic via tubulo-vesicular compartments[14-18], some of which were decorated with clathrin[19-21]. Moreover, tubulo-vesicular endosomes harboring the adaptors AP-1 and AP-3 as well as clathrin have been identified using immuno-EM, but were never characterized further[22,23]. These findings suggest that a tubulo-vesicular endosomal network may coordinate clathrin- and adaptor-dependent post-Golgi trafficking pathways, challenging the well-established vesicular transport model. Alternative mechanisms for organellar communications have also been proposed for other intracellular trafficking steps. Continuities between the endoplasmic reticulum (ER) and Golgi membranes have been shown to mediate export from the ER[24-26]. Correlation of light and electron microscopy images revealed an interwoven network of tubules, continuous with the ER mediating ER-Golgi transport, with COPII machinery localizing to the membranous connection between the two organelles[25]. Additionally, tubular structures connecting Golgi cisternae were observed[16].

Investigating the mechanisms and dynamics of proteins sorting out of the Golgi and within the endo-lysosomal system remains challenging, urging a combination of approaches aimed at investigating dynamic events and the underlying ultrastructure in near-physiological conditions. First, live-cell imaging is indispensable not only because of the transient and highly dynamic nature of many trafficking events[10], but also because post-Golgi structures, such as tubulo-vesicular compartments, are lost upon fixation[27]. Second, overexpression of fusion proteins, which is often used for making proteins accessible for live-cell imaging, holds the potential for artifacts[28,29], as too high protein levels can affect protein localization and function, making endogenous tagging crucial. Third, visualizing sorting events has been proven to be a difficult task in the perinuclear area where organelles are tightly packed, demanding super-resolution imaging techniques suitable for imaging live specimens[20,30,31]. Here, we utilize CRISPR-Cas9 technology to endogenously tag various sorting machinery components involved in post-Golgi trafficking with the self-labelling enzymes HaloTag and SNAP-tag[32]. Employing various imaging techniques, such as 3D correlative light electron microscopy, fast live-cell confocal and super-resolution STED microscopy, we were able to characterize novel multi-functional tubulo-vesicular ARF1 sorting compartment harboring

different adaptor proteins and clathrin. Trafficking assays and CRISPR-Cas9 mediated knock-outs point at a role for ARF1 compartments in endocytic recycling and secretory traffic where cargo is transferred from ARF1 compartments to recycling endosomes. Sorting machinery (AP-1, clathrin) is located at the interface where the two membranes interact and would facilitate cargo enrichment and transfer during kiss-and-run. Advancing previous thinking in this field, our findings suggest a model where cargo sorting would be mediated by a tubular network connecting the trans-Golgi network (TGN) with endo-lysosomes and the plasma membrane[13,33-35].

Results

Clathrin is associated with ARF1 compartments and organizes their fission

We recently identified TGN-derived tubulo-vesicular compartments defined by the small GTPase ARF1[20,27]. Interestingly, these compartments are decorated by clathrin nanodomains (Fig. 1A) and are observed in various cell types (Extended Data Fig. 1A-B) raising the possibility that they could be hubs for clathrin-coated vesicle budding or define a tubulo-vesicular network responsible for post-Golgi cargo sorting. When we applied super-resolution live-cell STED microscopy on ARF1^{EN}-Halo/SNAP-CLCa^{EN} (EN=endogenous) knock-in (KI) HeLa cells, we were able to highlight the close association of clathrin with ARF1 compartments (Fig. 1A). To test whether non-endocytic clathrin is exclusively associated with ARF1 compartments, we created an ARF1^{EN}-eGFP/Halo-CLCa^{EN}/AP2μ^{EN}-SNAP triple KI cell line (Fig. 1B). Quantification of clathrin association with either AP-2 (endocytic)[36] or ARF1 revealed that most of the non-endocytic clathrin decorates ARF1-positive membranes (Fig. 1C). Furthermore, we took advantage of fast confocal live-cell imaging to get a better understanding of the dynamics of clathrin on ARF1-compartments (Fig. 1D, Extended Data Video 1). Notably, we could not visualize any clathrin-coated vesicles budding from ARF1 compartments. Instead, we observed clathrin clusters translocating together with the closely associated membrane (Fig. 1E). Strikingly, when we looked at ARF1 compartments emerging from the TGN, we found clathrin associated with the detaching tubule (Fig. 1F). Without visualization of the underlying ARF1 membrane, these events could have easily been mistaken for a clathrin-coated vesicle moving within the cytoplasm or budding from the TGN. Intriguingly, clathrin localized at the fission site on ARF1 compartments, suggesting that clathrin and associated machinery may be responsible for the recruitment of fission factors. We analyzed more than 100 fission events and found that clathrin was present at >90% of the fission sites (Fig 1G-H, Extended Data Fig. 1C).

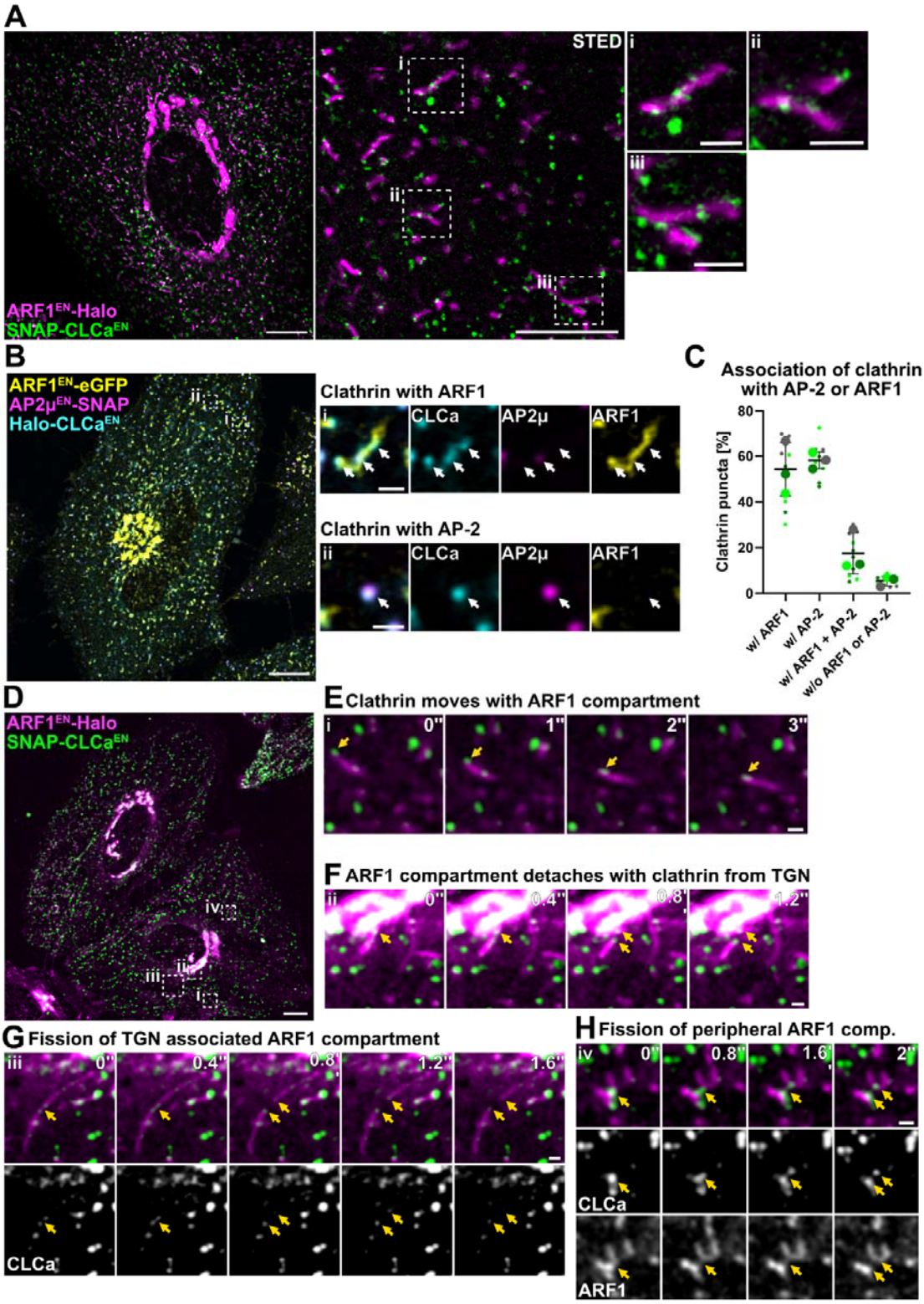

Figure 1: Fission of ARF1 tubules via association with non-endocytic clathrin coats.

(**A**) Live-cell confocal and STED imaging of ARF1^{EN}-Halo/SNAP-CLCa^{EN} HeLa cells labeled with CA-JF$_{571}$ and BG-JFX$_{650}$, show association of clathrin to ARF1 compartments. (**B**) Live-cell confocal imaging of ARF1^{EN}-eGFP/AP2μ^{EN}-SNAP/Halo-CLCa^{EN} HeLa cells labeled with CA-JF$_{552}$ and BG-JFX$_{650}$, highlighting association of (i) non-endocytic clathrin with ARF1 compartments and (ii)

endocytic clathrin with AP-2. (**C**) Quantification of clathrin-association with ARF1 and/or AP-2. In total 10 cells from 3 independent experiments were analyzed, replicates are shown in different colors and each small dot represents a single cell of the replicate. (**D**) Time-lapse confocal spinning disk imaging of ARF1^{EN}-Halo/SNAP-CLCa^{EN} HeLa cells labeled with CA-JF$_{552}$ and BG-JFX$_{650}$, (**E**) highlights movement of clathrin together with ARF1 compartments and (**F**) detachment of ARF1 compartments from the TGN together with clathrin. (**G**) Clathrin is found at sites of fission of ARF1 compartments when they detach from the TGN and (**H**) in the cell periphery. Selected frames are shown, movie was taken with a frame rate of 5 frames/s.
EN=endogenous, BG=benzylguanine (SNAP-tag substrate), CA=chloroalkane (HaloTag substrate)
Scale bars: 10 µm (confocal overview), 5 µm (STED image in **A**) and 1 µm (crops).

To get a better understanding of the membrane organization of ARF1 compartments and the association of clathrin with these membranes, we employed three-dimensional correlative light electron microscopy (3D-CLEM). ARF1^{EN}-Halo/SNAP-CLCa^{EN} KI cells were labeled with cell-permeable dyes and imaged post-fixation by scanning confocal microscopy (Fig. 2A), embedded, and a small region of interest was visualized using focused ion beam scanning electron microscopy (FIB-SEM) imaging (Fig. 2B). Alignment of confocal light microscopy and FIB-SEM imaging enabled the identification of ARF1 compartments at an isotropic resolution of 7 nm (Fig. 2Ci-iii). Intriguingly, the underlying tubulo-vesicular compartments displayed a pearled morphology that is reminiscent of the morphology of the ER-Golgi intermediate tubular compartments that mediate ER export[25]. In contrast to the clathrin-coated vesicular structures, which have a confined diameter between 70 and 90 nm, the diameter of the non-clathrin-coated ARF1 compartment varied between 20 nm and 180 nm (Fig. 2D). Clathrin-positive membranes seem to be preferably located at sites with high intrinsic curvature and are directly connected to the ARF1 compartment via a membranous neck (Fig. 2E). In summary, these data identify ARF1 compartments as the major site of clathrin-dependent intracellular sorting. This finding motivated us to further characterize the identity and function of these compartments.

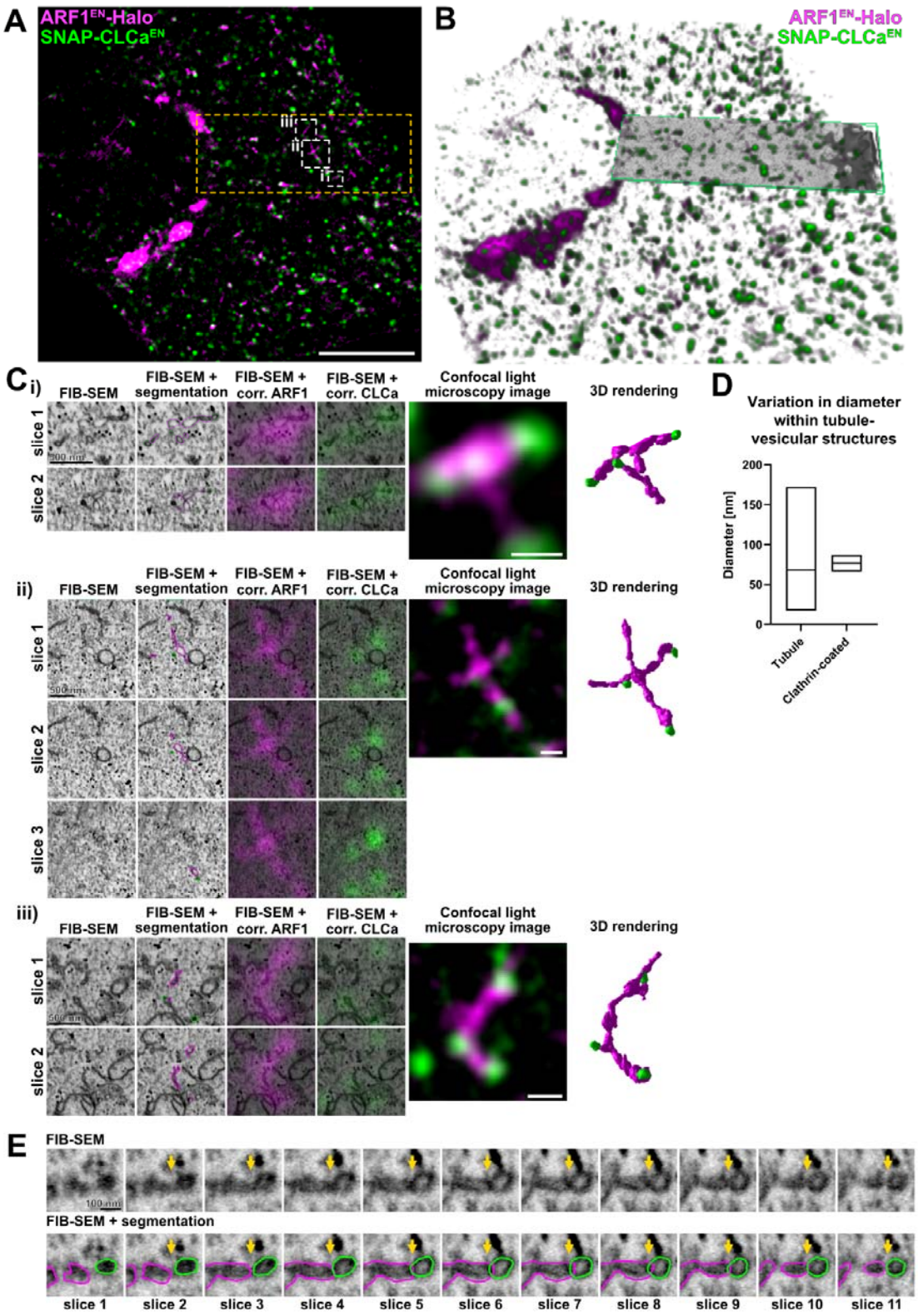

Figure 2: Tubulo-vesicular nature of ARF1 compartments revealed by 3D CLEM.

(A) Slice of a confocal z-stack of ARF1^{EN}-Halo/SNAP-CLCa^{EN} HeLa cell labeled with CA-JF$_{552}$ and BG-JFX$_{650}$ that was chosen for CLEM. The area that was imaged with FIB-SEM is highlighted with a yellow outline. Segmented ARF1 compartments (i-iii) are shown. (**B**) Overlay of the 3D projection of

the confocal stack and FIB-SEM image (green box). FIB-SEM image was obtained with 7 nm isotropic resolution. (**C**) Segmentation of individual ARF1 compartments with clathrin. Shown are 2-3 exemplary slices of the FIB-SEM image, the FIB-SEM image with outlines from the segmented area, overlays of fluorescence of ARF1 and clathrin with the FIB-SEM image, a representative slice of the confocal image of the ARF1 compartments and the 3D rendering from the ARF1 compartments. (**D**) Diagram showing variation in tubule diameter of the ARF1 compartment and the clathrin coated areas. Data for the diagram was obtained from the three ARF1 compartments shown in **C** that were measured at different parts of the tubule. (**E**) Single slices (7 nm increments) of the FIB-SEM data set, including segmentation, highlight the connection of clathrin-coated and non-coated part of the ARF1 compartment (arrow highlights neck of non-clathrin coated and clathrin coated ARF1 compartment).
Scale bars: 10 µm (overview in **A**), and 500 nm (crops in **C**).

AP-1 and AP-3 localize to segregated nanodomains on ARF1 compartments, clathrin is recruited to AP-1 (but not AP-3) positive nanodomains

Post-Golgi protein sorting relies on the recruitment of different cargo adaptors, such as AP-1 or AP-3 to membranes. Both adaptors were previously reported to localize to the TGN[6,8] and endosomal membranes[19,23,37], where they are implicated to coordinate bidirectional transport between TGN and endosomes (AP-1)[1,38,39] or transport to late endosomes and melanosomes (AP-3)[23,37]. As both adaptors are recruited by ARF1[3,4], we wondered whether they are present on ARF1 compartments. To test the localization of AP-1 and AP-3, we introduced a SNAP-tag to the C-terminus of their µA-subunit in ARF1^{EN}-Halo KI cells and created double KI cell lines (Fig. 3A-B). Interestingly, as observed for clathrin (Fig. 1A), live-cell STED highlighted nanodomains of both AP-1 and AP-3 on ARF1 compartments (Fig. 3A-B). We observed the same localization pattern when we endogenously tagged the large AP1γ1- or AP3δ1-subunit (Extended Data Fig. Fig. 2A-B). Simultaneous tagging of medium and large subunits showed both fusion proteins colocalizing within the same nanodomains, suggesting retained functionality (Extended Data Fig. 2C-D). In addition, AP-1-dependent clathrin recruitment was not affected by Halo-tagging of the µ-subunit (Extended Data Fig. 2E-F). As we observed both adaptors on ARF1 compartments, we asked whether these compartments represent multi-functional sorting endosomes responsible for both AP-1- and AP-3-dependent sorting or whether different classes of ARF1 compartments are defined by the different adaptors present. To understand the nature and function of the compartments, we created an ARF1^{EN}-eGFP/AP1µA^{EN}-Halo/AP3µA^{EN}-SNAP triple KI cell line (Fig. 3C). Live-cell confocal and STED imaging revealed that both adaptors localize to segregated nanodomains on ARF1 compartments and that the majority (~38%) of ARF1 compartments are decorated with AP-1 and AP-3 (Fig. 3C, Di, E). However, we could additionally observe ARF1 compartments that only supported AP-1 (~30%) or AP-3 recruitment (~10%) (Fig. 3Dii-iii, E). These data suggest that functionally distinct populations of ARF1 compartments may co-exist. About 20% of all ARF1 compartments did not harbor any AP-1 or AP-3, in agreement with a role for ARF1 tubules in retrograde Golgi-to-ER transport[20,27]. Both AP-1 and AP-3 were often shown to localize predominantly to the TGN/Golgi area in fixed cells[6,8]. However, in living gene-edited cells we found that only around 16% of total AP-1 and 6% of total AP-3 punctae were confined to the perinuclear area (Fig. 3F). Fixation is known to disrupt tubulo-vesicular cytoplasmic membranes[40] possibly leading to an overestimation of the fraction of Golgi-associated adaptors. Additionally, while a population of AP-1 punctae associated with the Golgi was very prominent, AP-3 was mainly excluded from the Golgi area (Fig. 3F). AP-4, the other adaptor protein complex recruited by ARF1[41], was predominantly associated with the Golgi (Fig. 3F, Extended Data Fig. 2G). These data suggest that ARF1 compartments serve as the main hub for AP-1 and AP-3-dependend sorting and might fulfill distinct intracellular functions based on the adaptors present.

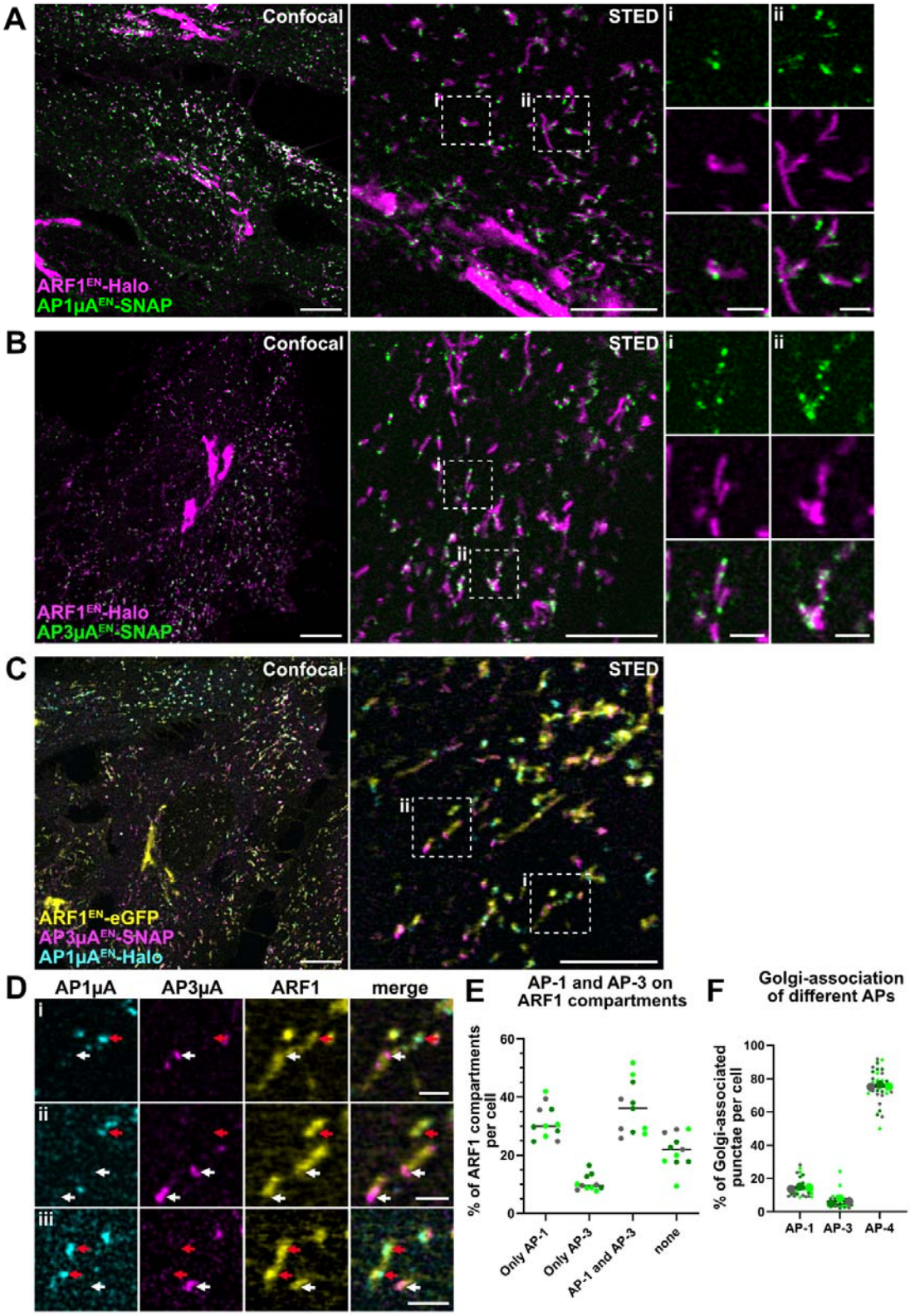

Figure 3: Adaptor protein complex AP-1 and AP-3 localize to segregated nanodomains on ARF1 compartments.

(**A-B**) Live-cell confocal and STED imaging of ARF1^{EN}-Halo/AP1μA^{EN}-SNAP HeLa cells (**A**) and ARF1^{EN}-Halo/AP3μA^{EN}-SNAP HeLa cells (**B**) labeled with CA-JF$_{571}$ and BG-JFX$_{650}$ show association of AP-1 and AP-3 to ARF1 compartments. **(C-D)** Live-cell confocal and STED imaging (2 color STED

imaging with ARF1^{EN}-eGFP imaged in confocal mode) of ARF1^{EN}-eGFP/AP3µA^{EN}-SNAP/AP1µA^{EN}-Halo HeLa cells labeled with CA-JF$_{571}$ and BG-JFX$_{650}$ show that AP-1 and AP-3 localize to segregated nanodomains on ARF1 compartments. (i) Crops highlight that AP-1 (red arrows) and AP-3 (white arrows) localize to segregated nanodomains on the same compartment. (ii-iii) In addition, ARF1 compartments with either AP-1 or AP-3 are found. (**E**) Quantification of the percentage of ARF1 compartments with specific adaptor identity per cell. In total 11 cells from 3 independent experiments were analyzed, replicates are shown in different colors each dot representing a single cell. (**F**) Quantification of Golgi-associated puncta positive for AP-1, AP-3 and AP-4. In total 30 cells from 3 independent experiments were analyzed for each condition, replicates are shown in different colors and each small dot represents a single cell of the replicate.
Scale bars: 10 µm (confocal overview), 5 µm (STED images) and 1 µm (STED crops).

Next, we wanted to investigate whether both AP-1 and AP-3 have the ability to recruit clathrin in living cells. Clathrin binding to AP-1 is well established[42]. Although AP-3 was shown to bind clathrin *in vitro*[6], the interaction of AP-3 with clathrin in mammalian cells is debated[23,43-46]. To resolve this issue, we created triple KI cell lines that allowed simultaneous visualization of ARF1, clathrin and AP-1 (ARF1^{EN}-eGFP/AP1µA^{EN}-SNAP/Halo-CLCa^{EN}) or AP-3 (ARF1^{EN}-eGFP/AP3µA^{EN}-SNAP/Halo-CLCa^{EN}) (Fig. 4A-D). Live-cell STED imaging of CLCa and AP1µA revealed a perfect colocalization of AP-1 and clathrin on ARF1 compartments (Fig. 4B). In contrast, AP-3 and clathrin localized to segregated nanodomains (Fig. 4D). Colocalization analysis shows a strong overlap between AP-1 and clathrin, whereas AP-3 and clathrin colocalization was similar to the negative control (AP-1 vs. AP-3, Fig. 4E). To further elucidate the role of AP-1 on ARF1 compartments, we created a CRISPR-Cas9 AP1µA knock-out (KO) in the ARF1^{EN}-Halo/SNAP-CLCa^{EN} KI cell line. Strikingly, loss of AP1µA led to the formation of elongated ARF1 compartments, suggesting a defect in fission (Fig. 4F). Clathrin recruitment to peripheral ARF1 compartments, but not to the Golgi, was impaired (Fig. 4G). Hence, AP-1 is responsible for the recruitment of clathrin and fission machinery to ARF1 compartments. Residual clathrin puncta were observed on ARF1 compartments (arrows in Fig. 4F) possibly suggesting recruitment via other clathrin adaptors such as GGAs (Golgi-localized, gamma-ear containing, ADP-ribosylation factor binding)[14,47].

To conclude, ARF1 compartments are multi-functional sorting endosomes harboring AP-1 and AP-3 nanodomains, with clathrin being recruited exclusively to AP-1 nanodomains. Beyond its role in cargo selection, AP-1 might also be required for the recruitment of fission factors.

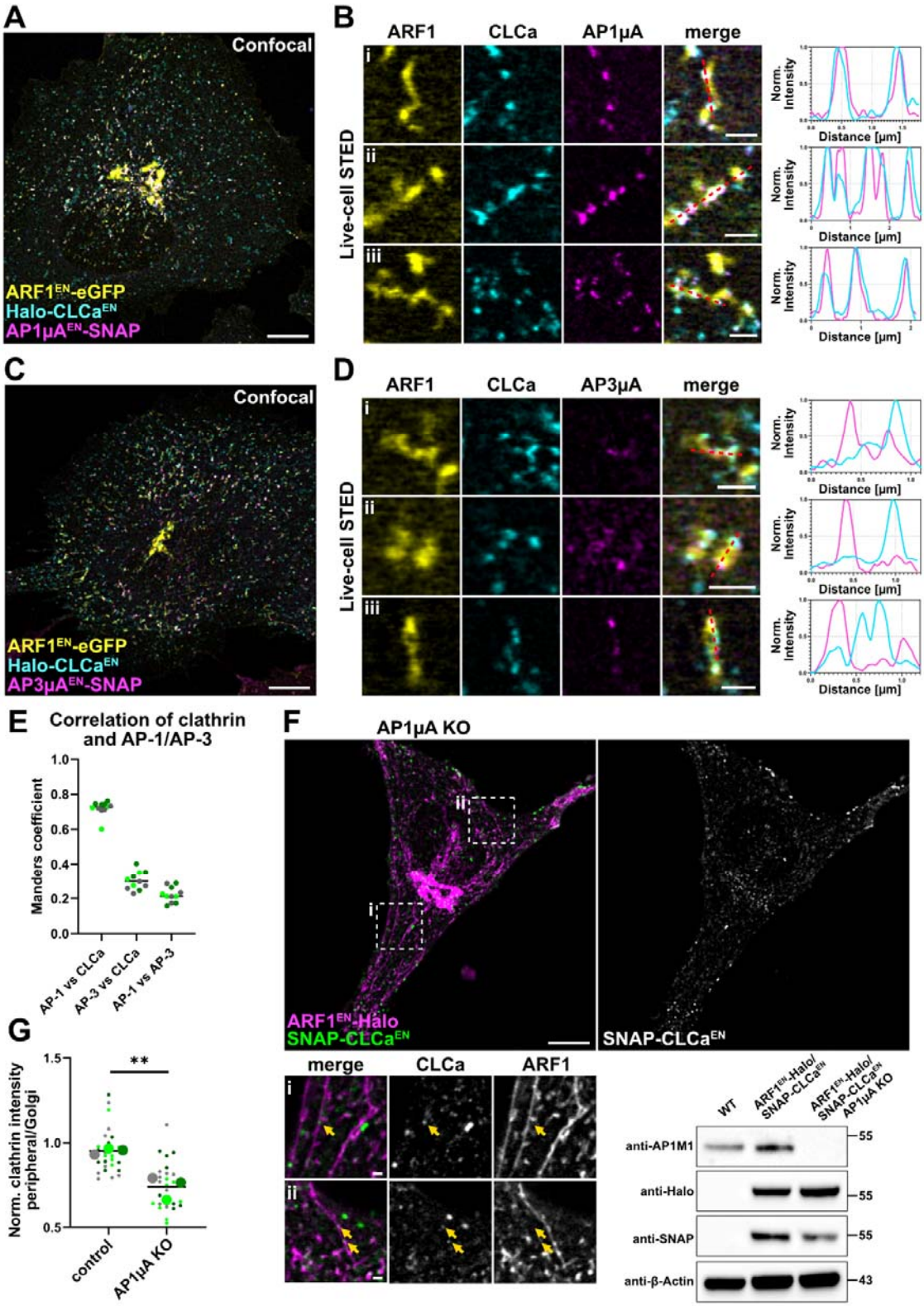

Figure 4: AP-1 but not AP-3 recruits clathrin to ARF1 compartments to mediate fission.

(**A-B**) Live-cell confocal and STED imaging (2 color STED imaging with ARF1^{EN}-eGFP imaged in confocal mode) of ARF1^{EN}-eGFP/AP1µA^{EN}-SNAP/Halo-CLCa^{EN} HeLa cells labeled with CA-JF$_{571}$ and BG-JFX$_{650}$ highlight that clathrin and AP-1 are recruited to the same nanodomains on ARF1 compartments. Line profiles of indicated lines in the STED crops show perfect colocalization of AP-1

with clathrin. (**C-D**) The same analysis on ARF1^{EN}-eGFP/AP3µA^{EN}-SNAP/Halo-CLCa^{EN} HeLa cells labeled with CA-JF$_{571}$ and BG-JFX$_{650}$ shows that clathrin and AP-3 do not colocalize on ARF1 compartments. (**E**) Colocalization analysis using the Manders coefficient shows high correlation of AP-1 with clathrin but low correlation of AP-3 with clathrin, comparable with the correlation of AP-1 with AP-3. In total 11 cells from 3 independent experiments were analyzed, replicates are shown in different colors each dot representing a single cell. (**F**) Live-cell confocal imaging shows that AP1µA KO in ARF1^{EN}-Halo/SNAP-CLCa^{EN} HeLa cells labeled with CA-JF$_{552}$ and BG-JFX$_{650}$ leads to the formation of aberrant long tubular ARF1 compartments. Clathrin recruitment to the long tubules seems to be reduced but not completely abolished (yellow arrows highlighted clathrin in crops i-ii). (**G**) Quantification of fluorescence intensity of clathrin punctae on peripheral ARF1 compartments normalized to the intensity of Golgi-associated clathrin punctae in control and AP1µA KO HeLa cells. In total 27 cells from 3 independent experiments were analyzed for each condition, replicates are shown in different colors and each dot represents a single cell of the replicate. P-value of nested t-test is 0.0064.
Scale bars: 10 µm (confocal overview), 5 µm and 1 µm (crops).

ARF1 compartments transiently interact with recycling endosomes (RE) via AP-1

We found ARF1 compartments to be hubs for adaptor-dependent post-Golgi sorting. As adaptors were described to associate with different endosomal compartments[19,23,38], we set out to investigate the nature of ARF1 compartments. For this, we visualized ARF1 in combination with known post-Golgi and endosomal membrane markers in live-cell confocal microscopy experiments (Fig. 5). First, we created a double KI cell line with Rab6, a membrane marker for tubular Golgi-derived carriers mediating direct transport to the plasma membrane[48], and found ARF1 and Rab6 to define different post-Golgi carriers (Fig. 5A). Next, to test whether ARF1 compartments are defined by early, late, sorting or RE markers, we created double KI cell lines of ARF1 with Rab7 (late endosome), SNX1 (sorting endosome) and Rab11 (recycling endosome) or transiently overexpressed Rab5 (early endosome). Live-cell confocal imaging revealed that ARF1 compartments were not defined by any of the tested membrane markers (Fig. 5A, white arrows highlight ARF1-only compartments). Interestingly, ARF1 compartments were observed in close proximity to Rab11-positive REs (Fig. 5A, yellow arrow) and fast confocal microscopy could highlight transient interactions of the same ARF1 compartment with different REs (Figure 5B, Extended Data Fig. 3A, Extended Data Video 2 and 3). To exclude any overlap between ARF1 compartments and REs we employed STED super-resolution microscopy. Live-cell STED revealed REs tethered to ARF1 compartments (Fig. 5C) and time-lapse STED imaging highlighted REs closely interacting with ARF1 tubules emerging from the TGN (Fig. 5Di, Extended Data Video 4) and cytoplasmic ARF1 compartments (Fig. 5Dii, Extended Data Fig. 3B, Extended Data Video 5). Fixed-cell STED z-stack imaging (Fig. 5Diii) showed multiple REs tethered to the same ARF1 compartments. To conclude, these data highlight ARF1 compartments as a novel post-Golgi sorting compartment that transiently interacts with RE.

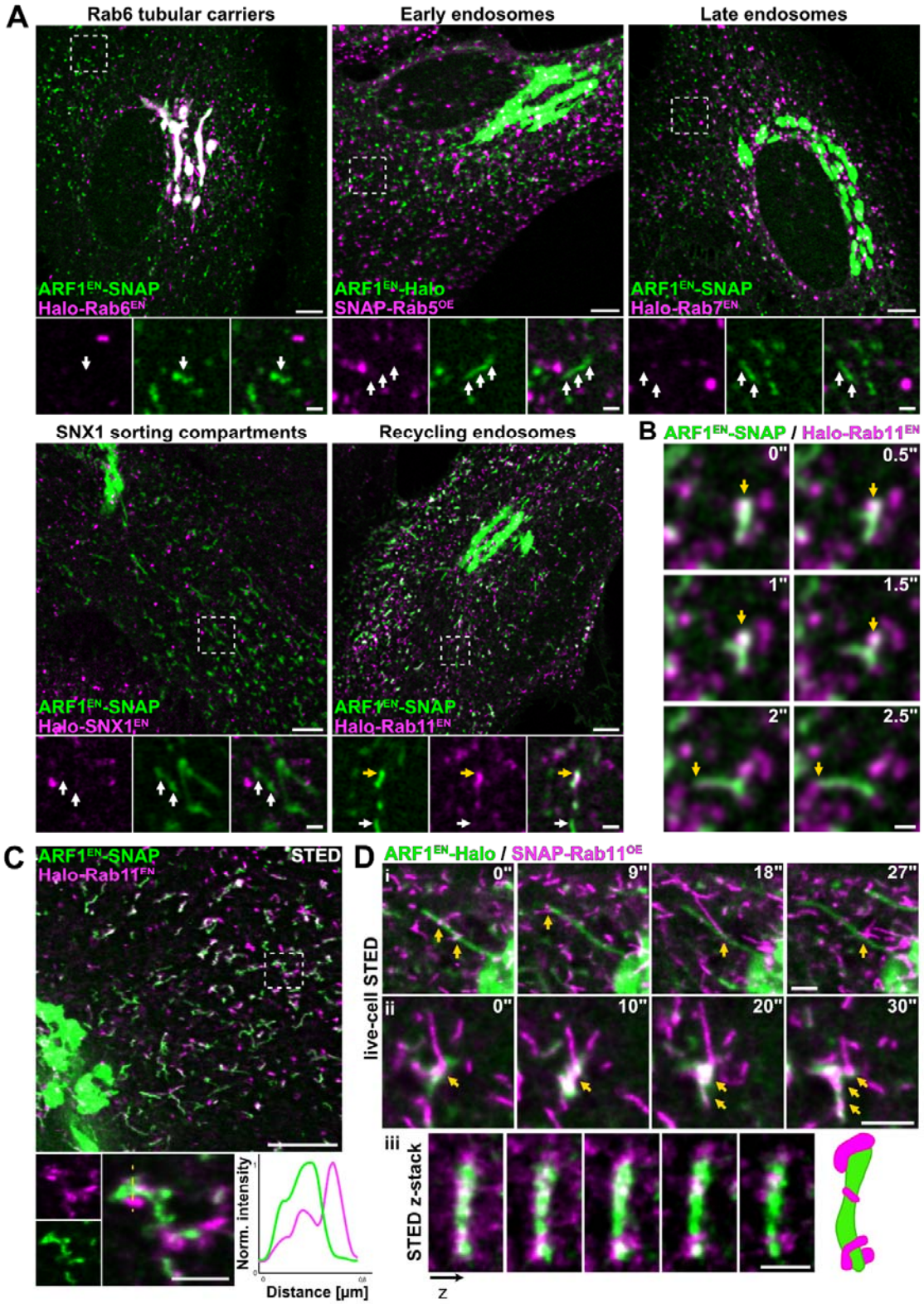

Figure 5. ARF1 sorting compartments are not defined by endosomal markers but interact with RE.

(**A**) Live-cell confocal microscopy of ARF1^{EN}-SNAP/Halo-Rab6^{EN} (Rab6 secretory carriers), ARF1^{EN}-SNAP/Halo-Rab7^{EN} (late endosomes), ARF1^{EN}-SNAP/Halo-SNX1^{EN} (SNX1 sorting compartment), ARF1^{EN}-SNAP/Halo-Rab11^{EN} (recycling endosomes) HeLa cells labeled with BG-JF$_{552}$ and CA-JFX$_{650}$ (ARF1+Rab6/7/11) or BG-JFX$_{650}$ and CA-JF$_{571}$ (ARF1+SNX1). ARF1^{EN}-Halo HeLa cells

transiently expressing SNAP-Rab5^{OE} were labeled with BG-JFX$_{650}$ and CA-JF$_{552}$. Imaging data highlight ARF1 compartments as a novel sorting compartment not colocalizing with any tested membrane markers (white arrows) but localizing closely to RE (yellow arrow). (**B**) Time-lapse confocal spinning disk imaging in ARF1^{EN}-SNAP/Halo-Rab11^{EN} HeLa cells labeled with CA-JFX$_{650}$ and BG-JF$_{552}$ shows ARF1 compartments transiently interacting with different REs. (**C**) Live-cell STED microscopy in ARF1^{EN}-SNAP/Halo-Rab11^{EN} HeLa cells labeled with CA-JF$_{571}$ and BG-JFX$_{650}$ highlights ARF1 compartments and REs at nanoscale resolution. Line profile analysis reveals close proximity of both compartments. (**D**) STED microscopy of ARF1^{EN}-Halo HeLa cells transiently expressing SNAP-Rab11^{OE} labeled with CA-JF$_{571}$ and BG-JFX$_{650}$ show the dynamic nature of the interaction of ARF1 compartments with REs (sites of interaction indicated with arrows) (i) at the TGN or (ii) in the cell periphery, (iii) fixed-cell 3D-STED microscopy highlights close proximity to multiple REs. OE=overexpression

Scale bars: 5 µm (overview) and 1 µm (crops, time-lapse and z-stack), Δz=0,2 µm.

The proximity between ARF1 compartments and REs prompted us to investigate whether cargo exchange may occur at the interface of both compartments and whether sorting machinery, such as AP-1, localizes where the two membranes are closely apposed. To investigate the spatio-temporal relationship between AP-1 on ARF1 compartments and REs, we created a triple KI cell line (ARF1^{EN}-eGFP/Halo-Rab11^{EN}/AP1µA^{EN}-SNAP). Live-cell confocal microscopy revealed that AP-1 is located on ARF1 compartments in close proximity to REs (Fig. 6A). Furthermore, time-lapse imaging showed AP-1 to be stably associated with moving ARF1 compartments. As ARF1 compartments closely interact with different REs (Fig. 6B, Extended Data Video 6), it may appear that AP-1 also associates with REs. Indeed, live-cell STED of Halo-Rab11^{EN}/SNAP-CLCa^{EN} KI cells also showed clathrin close to REs (Extended Data Fig. 4A). However, fast confocal imaging showed co-translocation of AP-1 with ARF1 compartments only (Fig. 6B) and quantification of the overlap between ARF1/AP-1/RE revealed a stronger association of AP-1 to ARF1 compartments compared to REs (Fig. 6C and Extended Data Fig. 4B). The localization of AP-1 at the interface between ARF1 compartments and REs suggests a role for AP-1 in cargo enrichment and transfer between closely interacting compartments. To perturb the possible function of AP-1 at the interface between the two membranes, we created an ARF1^{EN}-SNAP/Halo-Rab11^{EN} KI cell line lacking AP1µA and investigated the morphology of ARF1 compartments and REs with live-cell confocal microscopy. Strikingly, the absence of AP1µA led to the formation of long aberrant tubules positive for both markers (Fig. 6D-E), possibly derived from the fusion of the two compartments and/or membrane mixing. We speculate that, in addition to the role of AP-1 in cargo enrichment and transfer at membrane contacts, AP-1 may have an additional function in tethering and/or in the prevention of content mixing between ARF1 compartments and REs.

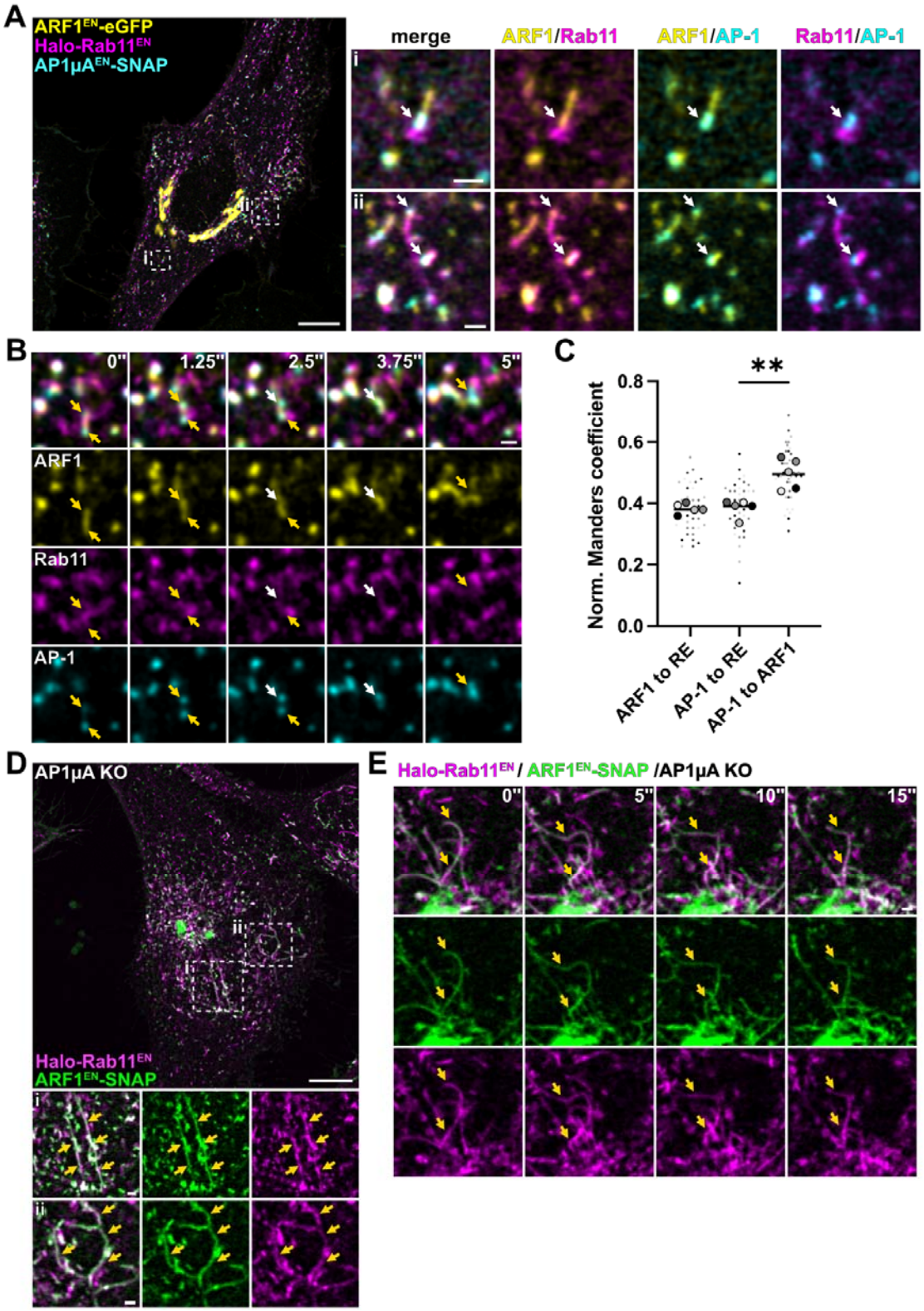

Figure 6. AP-1 nanodomains on ARF1 compartments are located at the interface with RE; loss of AP-1 KO results in morphological changes of both compartments.

(**A**) Live-cell confocal imaging of ARF1^{EN}-eGFP/Halo-Rab11^{EN}/AP1μA^{EN}-SNAP HeLa cells labeled with CA-JFX$_{650}$ and BG-JF$_{552}$ shows AP-1 at the interface of ARF1 compartment and RE. (**B**) Time-lapse confocal spinning disk imaging shows transient interaction of ARF1 compartments with different REs via AP-1. AP-1 seems to slide over the ARF1 compartment while interacting with

different REs (yellow arrows highlights AP-1 interacting with REs, white arrows show AP-1 without RE on ARF1 compartment). (**C**) Quantitative colocalization analysis between ARF1, AP-1 and RE. Normalized Manders coefficient shows comparable correlation of AP-1 to RE and ARF1 to RE, whereas correlation of AP-1 to ARF1 is significantly increased. Five replicates are shown in different colors each small dot representing a single cell of the replicate. P-value of the nested t-test is 0,0009. (**D**) Live-cell confocal imaging of ARF1^{EN}-SNAP/Halo-Rab11^{EN} AP1µA KO HeLa cells labeled with CA-JF$_{552}$ and BG-JFX$_{650}$, exhibit formation of long aberrant ARF1-compartments that show high colocalization with REs that show a similar aberrant elongation. (**E**) Time-lapse confocal microscopy of cells shown in **D** reveals joint movement of both compartments (ARF1 compartment and RE) over time.
Scale bars: 10 µm (confocal overview) and 1 µm (crops).

ARF1 compartments mediate endocytic recycling and secretory traffic via interaction with REs

So far, we have shown that ARF1-positive compartments are novel organelles that control clathrin and adaptor-dependent post-Golgi trafficking. To determine the exact role of ARF1 compartments in sorting, we investigated the trafficking of endocytic and secretory cargoes in different CRISPR-Cas9 KI and AP1µA KO cell lines. ARF1 compartments have been shown to mediate Golgi export of vesicular stomatitis virus glycoprotein (VSV-G)[20]. Interestingly, they were not observed fusing with the plasma membrane (PM) suggesting that another sorting step is required for the final delivery of VSV-G to the PM. We employed the Retention Using Selective Hooks (RUSH) system to release a pulse of secretory cargo from the ER[49]. The RUSH system consists of a reporter fused to a fluorescent protein or SNAP-tag that is retained in the ER by a streptavidin-KDEL hook. Upon biotin addition, the reporter is released from the ER and accumulates at the Golgi (~15 min) before reaching the PM (~30 min)[50]. We examined the secretory transport of two RUSH reporters: transferrin receptor (TfR, transmembrane protein) and TNFα (soluble cargo) with live-cell confocal microscopy in the various gene-edited cell lines. We found that both reporter cargoes exited the Golgi in ARF1/clathrin compartments (Fig. 7A-B, Extended Data Fig. 5A-B), e.g. moving away from the Golgi (Extended Data Fig. 5C-D). Furthermore, upon AP1µA KO, both TfR- and TNFα-RUSH were retained in long aberrant ARF1/Rab11 tubules (Extended Data Fig. 5E-G) and cargo exit from the TGN was delayed compared to control cells (Fig. 7C). Thus, AP-1 is required for TGN export of anterograde cargoes via ARF1 compartments.

REs have been shown to serve as an intermediate sorting station for secretory cargo exiting the Golgi *en route* to the PM[51,52]. Since ARF1 compartments do not fuse with the PM but closely interact with REs (Fig. 5), we tested whether secretory cargo is transported through RE. Therefore, we followed the transport of TfR-RUSH in Halo-Rab11^{EN} KI cells and found cargo colocalizing with REs (Fig. 7D). Moreover, three-color confocal live-cell imaging of TfR-RUSH, ARF1^{EN}-SNAP and Halo-Rab11^{EN} showed ARF1 compartments containing secretory cargo to be in close proximity to REs (Fig. 7E). We were further able to show that secretory cargo was handed over from ARF1 compartments to REs (Fig. 7F). Quantification of the kinetics of arrival of TfR-RUSH to ARF1 compartments and REs indicated the latter compartment to fill up following transit of cargoes through ARF1 compartments (Fig. 7G). Similarly, we observed ARF1 compartments with soluble cargo (TNFα-RUSH) interact with REs (Extended Data Fig. 5H). These results suggest a model in which ARF1 compartments that emerge from the Golgi subsequently hand over different secretory cargoes to REs.

As secretory cargoes were almost exclusively transported by perinuclear ARF1 compartments, we wondered about the function of peripheral ARF1 compartments that are devoid of anterograde cargo. AP-1 was previously shown to be important for transferrin (Tfn) recycling[53], motivating us to investigate the role of ARF1 compartments in endocytic

recycling. For this, we performed fluorescent Tfn uptake experiments in different gene-edited cell lines. After internalization, Tfn could be detected in peripheral ARF1 compartments (Fig. 7H) defined by AP-1 and AP-3 nanodomains (Extended Data Fig. 6A-C) before reaching REs (Fig. 7I, Extended Data Fig. 6D). Upon loss of AP1µA, Tfn export from ARF1 compartments was delayed (Fig. 7J). Intriguingly, Tfn was recycled through ARF1 compartments, which did not appear elongated as a result of the AP1µA KO, suggesting that AP-1 may only recruit fission factors on perinuclear compartments but not on peripheral recycling ARF1 compartments (Extended Data Fig. 6E). Lastly, to visualize endocytic and exocytic traffic through ARF1 compartments, Tfn uptake and TNFα-RUSH assays were simultaneously performed in $ARF1^{EN}$-Halo KI cells. Strikingly, ARF1 compartments located in the cell periphery were filled with endocytosed Tfn but were devoid of TNFα-RUSH anterograde cargo (Fig. 7Ki), while TGN-derived ARF1 compartments only contained TNFα-RUSH cargo (Fig. 7Kii).

Taken together, we suggest the presence of functionally different ARF1 compartments that coordinate endocytic recycling and secretory trafficking. Along both pathways, cargo appears to be handed over from ARF1 compartments to REs via AP-1.

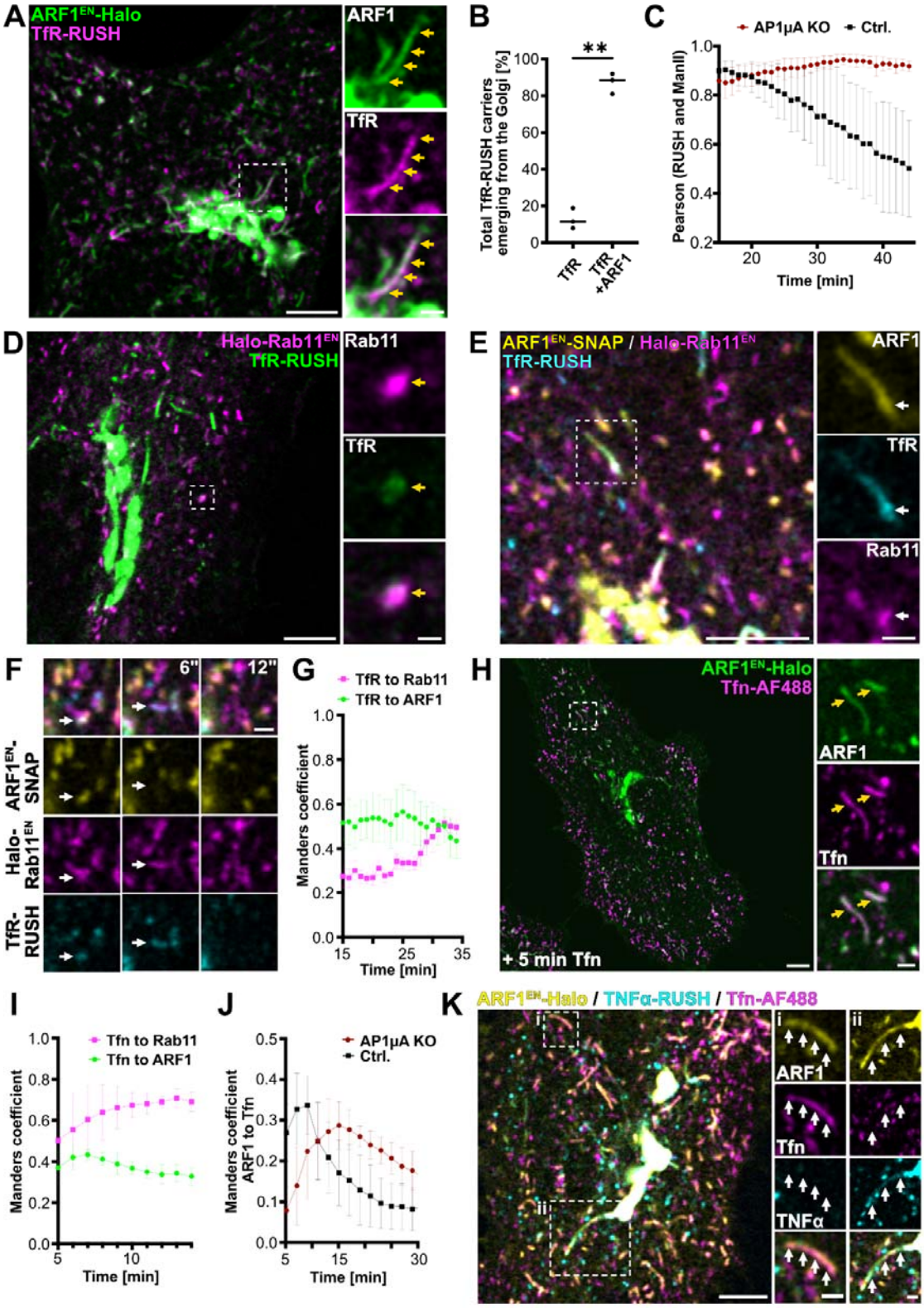

Figure 7. ARF1 compartments are involved in endocytic recycling and secretory trafficking; loss of AP-1 affects trafficking.

(**A**) ARF1^{EN}-Halo HeLa cells transiently expressing the RUSH construct Streptavidin-KDEL-TfR-SBP-SNAP labeled with CA-JF$_{552}$ and BG-JFX$_{650}$ were imaged with confocal microscopy 20 minutes after addition of biotin with a frame rate of 6 s/frame. A qualitative example shows secretory RUSH cargo leaving the Golgi in ARF1 compartments 21 minutes after addition of biotin. (**B**) Manual

quantification of the total TfR-RUSH tubules emerging from the Golgi reveals that most secretory RUSH cargo exits via ARF1 compartments, each dot represents a single cell, p-value is 0.0074. (**C**) Pearson correlation coefficient of secretory TfR-RUSH cargo and the Golgi (masked by the Golgi-marker ManII) reveals that upon AP1µA KO, Golgi exit of secretory cargo is impaired in comparison to control cells, each dot represents the average of 4 cells, SD error bars. (**D**) Live-cell confocal imaging of Halo-Rab11^{EN} HeLa cells transiently expressing Streptavidin-KDEL-TfR-SBP-GFP labeled with CA-JFX$_{650}$ shows that secretory RUSH cargo is sorted through REs *en route* to the PM. Image taken 21 minutes after addition of biotin. (**E**) Live-cell confocal image of ARF1^{EN}-SNAP/Halo-Rab11^{EN} HeLa cells transiently expressing Streptavidin-KDEL-TfR-SBP-eGFP labeled with CA-JF$_{571}$ and BG-JFX$_{650}$ highlights close proximity of ARF1 compartments filled with secretory RUSH cargo with a RE, 25 min after addition of biotin. (**F**) Confocal time-lapse imaging of cells prepared as in **E** shows transfer of RUSH cargo from an ARF1 compartment to a RE. (**G**) Colocalization analysis using the Manders coefficient shows that correlation of TfR-RUSH cargo with RE increases over time while correlation with ARF1 compartments slightly decreases. Each dot represents the average of 5 cells, SEM error bars. (**H**) Transferrin (Tfn) recycling assays were performed using fluorescently labeled transferrin (Tfn-AlexaFlour488). Live-cell confocal imaging in ARF1^{EN}-Halo HeLa cells labeled with CA-JFX$_{650}$ shows Tfn in ARF1 compartments 5 min after addition of Tfn. (**I**) Correlation analysis using the Manders coefficient of Tfn with ARF1 or Rab11 shows increasing correlation of Tfn with REs while correlation with ARF1 compartments slightly decreases over time. Each dot represents the average of 5 cells, SD error bars. (**J**) Correlation analysis using the Manders coefficient of ARF1 and Tfn in ARF1^{EN}-Halo HeLa cells or ARF1^{EN}-Halo/AP1µA KO HeLa cells shows that Tfn exits ARF1 compartments slower in AP1µA KO cells. Each dot represents the average of 5 cells, SD error bars. (**K**) Live-cell confocal imaging of ARF1^{EN}-Halo HeLa cells transiently expressing Streptavidin-KDEL-TNFα-SBP-SNAP labeled with BG-JFX$_{650}$ and CA-JF$_{552}$ shows that when performing both RUSH and Tfn recycling assay in parallel, both cargoes are in separate ARF1 compartments.
Scale bars: 5 µm (overviews) and 1 µm (crops).

Discussion

Clathrin-coated vesicles are thought to mediate cargo exchange between the TGN and different endosomal compartments as small punctate structures are commonly seen travelling around the cytoplasm of cells[6-9]. Endogenous tagging of ARF1 and clathrin together with CLEM allowed us to visualize the membrane underlying clathrin-positive vesicle-like structures and revealed that the vast majority of non-endocytic clathrin is associated with a tubulo-vesicular network of ARF1 compartments (Fig. 1-2). ARF1 compartments do not possess the identity of common endosomal makers (Fig. 5), suggesting a novel tubulo-vesicular organelle with a key role in distribution of cargo along post-Golgi routes. Clathrin translocates and remains associated with ARF1 compartments, and no budding events were observed (Fig. 1). However, visualization of budding events from moving objects is technically challenging and would require fast volumetric imaging to detect rapid uncoating events after vesicle formation.

ARF1 compartments organize secretory cargo export from the TGN as well as recycling to the PM by handing over cargo to REs (Fig. 7). The molecular machinery (AP-1 and clathrin), which mediates cargo selection and transfer localizes at the interface between the two membranes (Fig. 6). Based on these observations, we speculate that AP-1 may coordinate short-range cargo transfer between the two organelles. This could occur either via recognition of the membranes in *trans*, followed by short-range vesicular transport, or via a kiss-and-run mechanism (Fig. 8). In the case of a transient pore or membrane bridge formation, we speculate that AP-1 could enrich and select cargo, while at the same time concentrate tethering molecules and/or act as a diffusion barrier. A novel additional function for coats in providing a diffusion barrier at the level of membrane continuities has also been speculated for COPII at the neck of ER exit sites[25]. Alternatively, AP-1 could also have a role in concentrating tethering factors[54] at the site of kiss-and-run, and absence of AP-1 would lead to tethering of Rab11 endosomes over the length of the tubules (Fig. 6D-E). Similarly, aside from its ability to induce membrane curvature, clathrin might be required for the clustering of AP-1 at sites of cargo exchange, as the lack of clathrin leads to diffused localization of AP-1 along tubular structures[55].

The presence of AP-1 and AP-3 nanodomains on ARF1 compartments involved in Tfn recycling (Extended Data Fig. 5) tempts us to speculate that AP-3 could, in a similar manner, drive interaction and transfer of endocytosed proteins to endo-lysosomes. This would build on the emerging idea of a tubular endosomal network (TEN), which transiently exchanges cargoes with various endosomal compartments and transport carriers via kiss-and-run, thus mediating sorting of endo-lysosomal proteins[13]. AP-3 is reported to act in sorting from endosomes to melanosomes but its role in non-specialized cells is controversial[37]. Generally, AP-3 might be involved in the sorting of lysosomal cargoes as LAMP1 is mistargeted in AP-3 deficient mice[56], calling for further investigation on the role of ARF1 compartments in transport to lysosomes. Although it was speculated that AP-3 does not bind clathrin *in vivo*[43,44], the presence of a clathrin box in the β-subunit of AP-3 as well as its ability to bind clathrin *in vitro* indicated a possible AP-3/clathrin interaction[6]. Interestingly, we only see association of clathrin with AP-1 but not with AP-3, indicating that AP-3 and clathrin do not interact *in vivo*.

AP-1 is a versatile adaptor that acts in many trafficking steps. Because of this plethora of functions in many different cell types, it has been difficult to reach a consensus about the core functions of AP-1. AP-1 is thought to coordinate bi-directional transport between the TGN and endosomes[1,38,39]. In yeast, an additional role for AP-1 in intra-Golgi recycling of Golgi-resident proteins has also been suggested[57]. Our data suggests that different sub-populations of ARF1/AP-1 compartments could coordinate different intracellular trafficking steps. While perinuclear ARF1 compartments are important for TGN export and secretory transport, peripheral ARF1 compartments mediate endocytic recycling. Upon AP1µA KO we observed defects in TGN cargo export (Fig. 7) and formation of TGN-derived aberrant

elongated ARF1 compartments (Fig. 4). The defect in TGN export could be explained by a defect in the retention of TGN-resident proteins or possibly a defect in retrograde endosome-to-Golgi recycling[39]. As for the fission defects, we speculate AP-1 is responsible for the recruitment of yet-to-be identified fission factors. A potential role for the membrane-remodeling GTPase dynamin in fission events at the TGN is controversial, as several approaches suggested a contribution of dynamin to the fission of clathrin-coated vesicles from the TGN and endosomes[17,58,59], while *in vivo* studies show that it exclusively promotes fission of endocytic vesicles[60,61]. Interestingly, ARF1 has been proposed to mediate dynamin 2 recruitment, and depletion of dynamin 2 led to long tubular extensions from the TGN[58], reminiscent of the elongated ARF1 compartments we observe upon AP-1 depletion. Additionally, we find AP-1 on ARF1 compartments involved in the recycling of endocytosed cargo proteins, where AP-1 would facilitate protein transfer to REs for PM delivery. Interestingly, peripheral ARF1 compartments involved in Tfn recycling remain morphologically unchanged upon AP1µA KO, while Tfn recycling is defective (Fig. 7, Extended Data Fig. 6)[53]. While the cargo enriching and sorting functions of AP-1 may be conserved, differential recruitment and specific function of AP-1 may be driven by distinct subsets of interacting proteins and co-adaptors, including specific lipid-modifying enzymes such as phosphatidylinositol-4-kinases[62]. Loss of AP1µA led to a pronounced reduction of clathrin association on long aberrant ARF1 compartments, without affecting clathrin recruitment to the Golgi (Fig. 4F-G). Clathrin could be recruited to ARF1 compartments or the TGN via other ARF-dependent adaptors such as GGA proteins[39,63]. Sub-populations of AP-1, either associated with GGAs or alone could drive differential effector recruitment. Additionally, the role of non-classic adaptor proteins, such as EpsinR[64], in intracellular clathrin-dependent sorting is little explored.

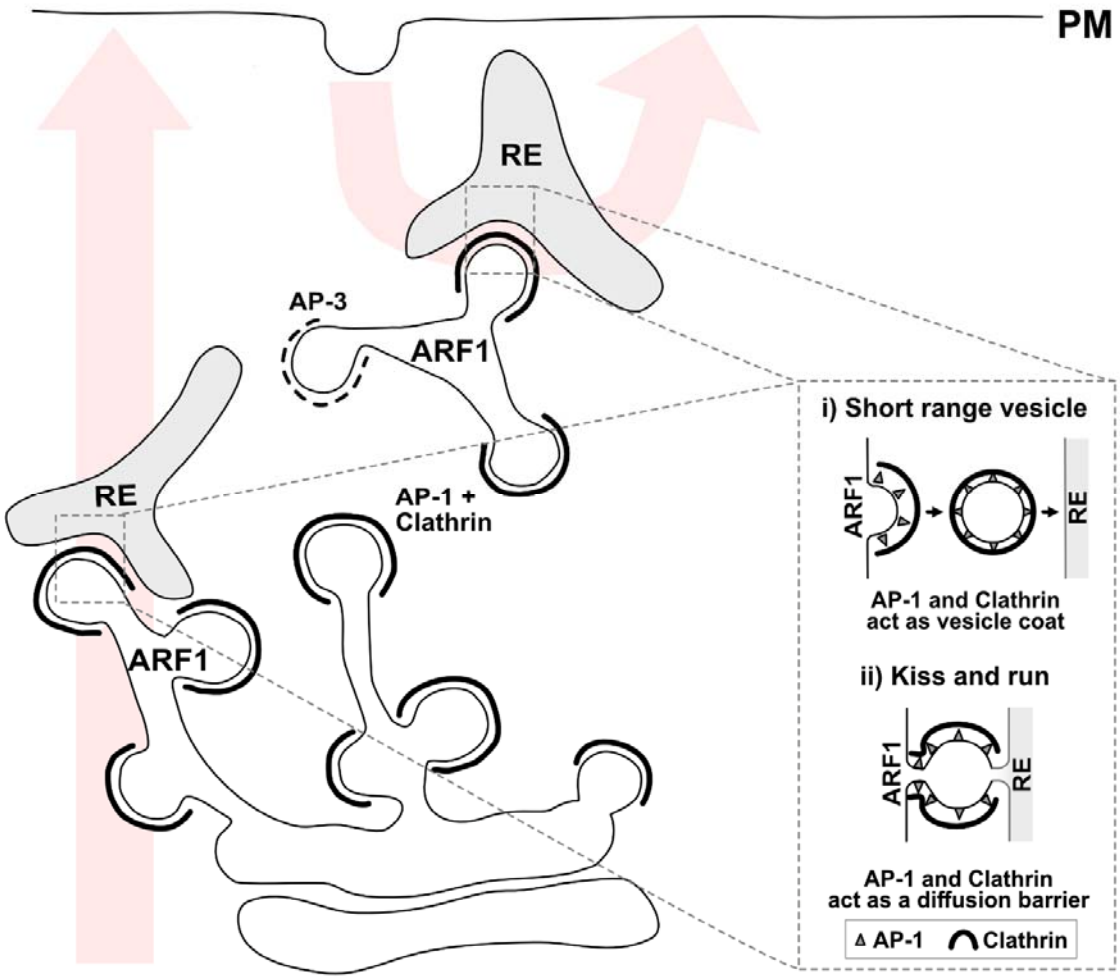

Figure 8. Model of the function of ARF1 compartments in secretory and endocytic recycling cargo sorting. ARF1 compartments harbor nanodomains of AP-3 and AP-1/clathrin allowing for site-specific cargo enrichment. AP-1-dependent cargo is transferred from ARF1 compartments to RE by (i) formation of short-range clathrin-coated vesicles or (ii) transient interaction via kiss-and-run.

We could observe tubulo-vesicular ARF1 compartments decorated with clathrin in different mammalian cell types (Extended Data Fig. 1), hinting at a conserved mechanism for post-Golgi transport via ARF1 compartments. Recently, cargo exchange between RE and SNX1-positive sorting endosomes was described in *C.elegans* and mammalian cells[11], fueling the idea of a conserved mechanism for short-range cargo transfer across species via kiss-and-run. Further support comes from work in *Drosophila*, where direct transient interaction of TGN with RE has been observed for cargo sorting[65]. As the organization of the endosomal system differs strongly between organisms and cell types, due to the presence of specialized endosomes and distinct metabolic needs, we expect cell type-dependent variations of the here described mechanism[66]. ARFs are abundant and ubiquitously expressed proteins in all organisms, suggesting their key role in post-Golgi trafficking may be conserved. Diversity of function in different cell types and organisms might also be driven by the presence of different adaptors and effector proteins. In polarized epithelia cells, the tissue-specific adaptor AP-1B is additionally expressed[67], adding another layer of complexity to the sorting process.

Overall, by using advanced imaging methods to visualize endogenously labelled sorting machinery, we provide evidence for intracellular material exchange being facilitated by a tubulo-vesicular network that connects the TGN, the endosomal system and the PM.

Methods

Mammalian cell culture

CCL-2 HeLa cells (ECACC General Collection) and HAP1 cells[68] were grown in a humidified incubator at 37°C with 5% CO_2 in Dulbecco's Modified Eagle Medium (DMEM, Gibco) supplemented with 10% fetal bovine serum (Corning), 100 U/L penicillin and 0.1 g/L streptomycin (FisherScientific). Jurkat T-cells (ECACC General Collection) were grown in a humidified incubator at 37°C with 5% CO_2 in Roswell Park Memorial Institute medium (RPMI, Gibco) supplemented with 10% fetal bovine serum (Corning), 100 U/L penicillin and 0.1 g/L streptomycin (FisherScientific).

For transient transfection of plasmids encoding for SNAP-Rab5, GFP-ManII or RUSH cargoes into HeLa cells, a NEPA21 electroporation system was used (Nepa Gene). For this, 1 million cells were washed twice with Opti-MEM (Gibco), resuspended in 90 µl Opti-MEM and mixed with 5 µg for SNAP-Rab5, 1 µg for ManII-GFP, 10 µg for RUSH cargo of DNA in an electroporation cuvette with a 2-mm gap. The electroporation reaction consists of two poring pulse (125 V, 3 ms length, 50 ms interval, with decay rate of 10% and + polarity) and five consecutive transfer pulse (25 V, 50 ms length, 50 ms interval, with a decay rate of 40% and ± polarity).

Recombinant plasmids for overexpression

See supplementary information.

CRISPR-Cas9 KI and KO plasmids and cell lines

See supplementary information.

Live-cell labelling

For live-cell imaging, cells were seeded on a glass-bottom dish (3.5 cm, #1.5; Cellvis) coated with fibronectin (Sigma). Labeling with Halo and SNAP substrates was carried out for 1 h at 37°C in culture media. All dyes-conjugates were used at concentration of 1 µM. After the staining, cells were washed in growth media at 37 °C for at least 1 h. Live-cell imaging was performed in live-cell imaging solution (FluoBrite DMEM (Gibco) supplemented with 10% FBS, 20 mM HEPES (Gibco) and 1x GlutaMAX (Gibco)).

For live-cell labeling of non-adherent T-cells, 200 000 cells were labeled with Halo and SNAP substrates (1µM) for 1 h at 37ºC in culture media in a volume of 100µl. After staining, cells were washed in growth media 3 times via centrifugation.

Imaging and image processing

Line-scanning confocal and STED imaging was carried out on a commercial expert line Abberior STED microscope equipped with 485 nm, 561 nm and 640 nm excitation lasers. For two-color STED experiments both dyes were depleted with a 775 nm depletion laser. The detection windows were set to 498 to 551 nm, 571 to 630 nm and 650 to 756 nm. Multi-color STED images were recorded sequentially line by line. For confocal imaging, probes that were detected in the 498 to 551 nm and the 650 to 756 nm detection windows were recorded simultaneously. If required for quantitative analysis, laser power was kept constant between images. For live-cell confocal imaging the pixel size was set to 60 nm and for STED imaging to 30 nm (live-cell) or 20 nm (fixed cell). Live-cell imaging was performed at 37ºC.

Spinning disk confocal imaging was carried out at CSU-W1 SoRa spinning disk (Nikon) with a dual camera system for simultaneous dual-color detection. All imaging was performed with a 60x Plan Apo oil objective (NA=1.4). For experiments 488 nm, 561 nm and 636 nm laser

lines were used for excitation. For simultaneous dual color imaging, the quad-bandpass filter was used with relevant center wavelengths of 607 nm and 700 nm and full-width half maximums of 34 nm and 45 nm, respectively. For three-color imaging, eGFP and far-red (JFX_{650}) signal were detected simultaneously, and the orange channel (JF_{552}) was detected separately. Again, the quad-bandpass filter was used with relevant center wavelengths of 521 nm, 607 nm and 700 nm and full-width half maximums of 21 nm, 34 nm and 45 nm, respectively.

To reduce noise, confocal images were background subtracted and gaussian blurred (1 pixel SD) using Fiji[69]. STED images in Fig. 5 were deconvoluted using Richardson–Lucy deconvolution from the python microscopy PYME package (https://python-microscopy.org). Line profiles shown in Fig. 4B, D and Fig. 5C were obtained by drawing a perpendicular line to the direction of the membrane with Fiji on gaussian blurred (1 pixel SD) STED images. The line profile data was then normalized and plotted using GraphPad Prism (GraphPad Software, https://www.graphpad. com).

FIB-SEM CLEM

For 3D CLEM, ARF1^{EN}-Halo/SNAP-CLCa^{EN} HeLa cells were grown on IBIDI gridded glass coverslips. Cells were stained with SNAP-tag and HaloTag substrates as for standard light microscopy. Additionally, lysosomes were labeled SiX-lysosome[70] (0.5 µM) after Halo- and SNAP-labelling was complete, to visualize lysosomes. Cells were fixed for 15 min at 37°C using 3% PFA and 0.2% glutaraldehyde. Following the fixation, the reaction was quenched using 0.1% $NaBH_4$ in PBS for 7 min and cells were rinsed three times with PBS afterwards. Cells were then directly imaged in PBS. From chosen cells confocal z-stacks with 200 nm increments were recorded. All three colors were recorded sequentially line-by-line.

Following light microscopy, cells were postfixed with 2% glutaraldehyde in 0.1 M cacodylate buffer. Osmification was performed with 1% OsO4 and 1.5% potassium cyanoferrate (III) in 0.1 M cacodylate buffer on ice, followed by aqueous 1% OsO4 at room temperature. Following washing, 1% uranyl acetate was applied and dehydration in ascending ethanol concentration was performed. Ultrathin embedding into Durcupan resin was performed[71]. After centrifugation of excessive resin amount, coverslips with cells were put into the heating cupboard for polymerization.

Following resin polymerization, coverslips were trimmed with a glass cutting pen and mounted onto SEM pin stabs, sputter coated with carbon (30-50 nm) and imaged in SEM (Helios 5CX). Low-resolution overviews of coverslip surface were used to navigate on the coverslip and find the corresponding quadrant with the cell of interest. Sum projection image from SDCM was overlaid with a SEM cell image (ETD, secondary electrons) in Thermofischer MAPS software to specify part of cell for autoslice and view (ASV). FIB milling was performed at 7 nm step, SEM imaging was performed at x = 3.37 nm; y = 4.6 nm, dwelling time 5 µs, backscattered electrons were detected by in-Column detector at 2kV, 0.34 nA.

Stack alignment was performed in freeware Microscopy image browser (MIB). 3D stacks were binned to 7 nm isotropic resolution and further CLEM alignment, feature segmentation and visualization was performed using Dragonfly software. In short, SiX-labeled lysosomes were used for rough alignment, fine alignment of light microscopy and electron microscopy volumes was performed by orienting on cell membrane edges and plasma membrane coated pits, that were clearly visible in FIB stack as well as light microscopy. Following alignment, numerous ARF1 stained tubules were inspected and all of them are correlated with corresponding tubular compartment in electron microscopy images. ARF1 compartments and

clathrin coated compartments were segmented manually. Diameter of compartments and clathrin-coated membranes (Fig. 2D) was measured using the ruler tool in Dragonfly. The diameter of ARF1 compartments was measured in irregular distances within the ARF1 compartments shown in Fig. 2.

Fixed-cell STED Z-stack

To preserve tubular-vesicular structures for acquisition of 3D z-stack (Fig. 5Diii), cells were fixed with 3% PFA and 0.2% glutaraldehyde, as described for FIB-SEM CLEM fixation. The z-stack was recorded with 200 nm increments.

Trafficking assays

For the RUSH assay (Fig. 7A-G, Extended Data Fig. 5), plasmids encoding for the different RUSH cargoes as described in the figure legend were transiently transfected into HeLa cells and seeded on fibronectin coated microscopy dishes. 18 h after transfection, cells were stained with live-cell imaging dyes. The biotin stock solution (c=585 mM in DMSO) was diluted to a final concentration of 500 µM (in live-cell imaging solution) before addition to the cells. Live-cell confocal imaging was started 15 min or 20 min post biotin addition to investigate post-Golgi trafficking of the cargo.

For the Tfn assays (Fig. 7H-J, Extended Data Fig. 6), live-cell labeled HeLa cells were put on ice for 10-15 min before incubated with Tfn-AF488 (25 µM, ThermoFisher) in live-cell imaging solution at 37°C for 3 min. Cells were washed once with live-cell imaging solution before live-cell imaging with holo-Tfn (1 mM, ThermoFisher) was added to prevent re-endocytosis of labeled Tfn.

For the simultaneous RUSH and Tfn uptake assay (Fig. 7K), cells were prepared for the RUSH assay as described above. Live-cell imaging solution containing biotin was added to the cells (final concentration biotin= 500 µM) for 12 minutes at 37°C allowing it to pulse the secretory RUSH cargo out of the ER. Then, the medium was changed to live-cell imaging solution containing Tfn-AF488 (final concentration= 50 µM) for 30 s at 37°C allowing Tfn entry into the cell followed by live-cell imaging.

Image Quantification

Prism was used to generate all graphs and to calculate SD and SEM. Data sets containing continuous data from different biological replicates were presented as superplots[72].

To estimate the association of clathrin with ARF1 compartments and AP-2 (Fig. 1C), all clathrin punctae were manually counted in 10 ARF1^{EN}-eGFP/AP2µ^{EN}-SNAP/Halo-CLCa^{EN} HeLa cells from 3 independent experiments and categorized in 3 categories depending on their colocalization with either ARF1 or AP-2 or neither of them. A fourth category (ARF1+AP-2) shows the percentage of clathrin puncta which association could not be unambiguously determined. From each cell, an image at the Golgi plane and an image at the apical plasma membrane was acquired and used for quantification. For quantification of ARF1 compartments with different adaptor identity (Fig. 3D) ARF1^{EN}-eGFP/AP1µA^{EN}-SNAP/AP3µA^{EN}-Halo HeLa cells were analyzed manually. Compartments were categorized based on which AP was found associated with the structure.

To estimate the amount of association of different APs with the Golgi, dual color confocal images of ARF1^{EN}-Halo/AP1µA^{EN}-SNAP, ARF1^{EN}-Halo/AP3µA^{EN}-SNAP and ARF1^{EN}-Halo/AP4µ^{EN}-eGFP HeLa cells were used for the analysis in Fiji. A mask of the Golgi was drawn using the ARF1-signal as reference. Using the “Find Maxima”-Tool of Fiji the number

of AP puncta in the Golgi area and in the entire cell measured to estimate the percentage of Golgi associated AP.

To quantify the correlation of clathrin with AP-1 and AP-3 (Fig. 4E) the Manders correlation coefficient was used. Confocal images of ARF1^{EN}-eGFP/AP1µA^{EN}-SNAP/Halo-CLCa^{EN}, ARF1^{EN}-eGFP/AP3µA^{EN}-SNAP/Halo-CLCa^{EN} and ARF1^{EN}-eGFP/AP1µA^{EN}-SNAP/AP3µA^{EN}-Halo HeLa cells were background subtracted, gaussian blurred and the cell was selected as ROI. After automatic thresholding with Fiji the Manders correlation coefficient was determined.

To estimate the change in clathrin recruitment upon AP1µA KO (Fig. 4G), confocal images of ARF1^{EN}-Halo/SNAP-CLCa^{EN} and ARF1^{EN}-Halo/SNAP-CLCa^{EN} AP1µA KO HeLa cells were analyzed. Each cell was imaged at the plasma membrane plane and the Golgi plane. In each cell the fluorescence intensity of 10 clathrin puncta which were associated with ARF1 compartments were measured and averaged. For normalization, the average intensity of 10 clathrin plaques at the plasma membrane was used.

The correlation of ARF1, Rab11 and AP-1 in Fig. 6C was investigated by live-cell confocal imaging of ARF1^{EN}-eGFP/Halo-Rab11^{EN}/AP1µA^{EN}-SNAP HeLa cells labeled with CA-JFX$_{650}$ and BG-JF$_{552}$ by taking square confocal images of the cytosol. The images were background subtracted and gaussian blurred and thresholded with Fiji before determining the Manders correlation coefficient with the JaCOP Fiji PlugIn[73]. To avoid higher values due to coincidental overlap, the obtained Manders values were subtracted by the Manders value measured once one channel is rotated by 90 degrees revealing the normalized Manders values shown in Fig. 6C.

To quantify the percentage of secretory tubules exiting the Golgi positive for ARF1 (Fig. 7B), RUSH assays were performed in ARF1^{EN}-Halo HeLa cells transiently overexpressing Streptavidin-KDEL-TfR-SBP-SNAP labeled with CA-JF$_{552}$ and BG-JFX$_{650}$. Live-cell confocal time lapses were taken 20 minutes post biotin addition at 6 s/frame imaging speed. Tubules emerging from the Golgi were counted manually from 3 different cells.

For determining the Golgi export delay upon AP1µA KO (Fig. 7C), RUSH assays were performed in ARF1^{EN}-Halo (control) or ARF1^{EN}-Halo AP1µA KO HeLa cells transiently overexpressing Streptavidin-KDEL-TfR-SBP-SNAP and ManII-GFP (Golgi mask) labeled with BG-JFX$_{650}$. Live-cell confocal overview images were taken 15 min post biotin at 1 min/frame. The ROI was selected by hand excluding the nucleus and the Pearson correlation coefficient over time was determined using the JaCOP plugin of Fiji.

To understand the directionality of secretory cargo transfer between ARF1 compartments and RE (Fig. 7G), RUSH assays of Streptavidin-KDEL-TfR-SBP-SNAP transiently overexpressed in ARF1^{EN}-Halo or Halo-Rab11^{EN} HeLa cells were performed. Images were captured 15 min post biotin at 1 min/frame. Confocal images were background subtracted, gaussian blurred and the ROI was selected by hand excluding the nucleus and Golgi. The threshold was obtained for every channel with Fiji and then Manders values were determined with the JaCOP plugin.

To understand the directionality of endocytic recycling cargo transfer between ARF1 compartments and RE (Fig. 7I), Tfn assays were performed in ARF1^{EN}-SNAP/Halo-Rab11^{EN} HeLa cells labeled with CA-JFX$_{650}$ and BG-JF$_{552}$. Overview images were captured 5 min post internalization at 1 min/frame. The Manders was determined as for Fig. 7G.

To quantify the effect of an AP1µA KO on Tfn trafficking (Fig. 7J), Tfn assays were performed in ARF1^{EN}-Halo and ARF1^{EN}-Halo AP1µA KO HeLa cells labeled with CA-JFX$_{650}$. Tfn recycling was recorded every 2 min for 30 min and the Manders correlation coefficient of ARF1 and Tfn was determined for every time point.

Antibodies and Dyes

All live-cell imaging dyes used in the study are indicated in the figure legends and were provided from the Lavis lab[74,75]. All antibodies used in this study are provided in Supplementary Table 4.

Acknowledgments

This project was supported by the Deutsche Forschungsgemeinschaft (German Research Foundation) grants SFB958 (Project A25) and SFB/TRR186 (Project A20). C.R. is supported by a Human Frontier Science Program (HFSP) early career award to F.B.. We thank Luke Lewis (Janelia Research Campus) for providing all live-cell dyes we used in this study and Alexey Butkevich (Max Planck Institute for Biophysical Chemistry) for providing the SiX-lysosomal probe. We are grateful to David Gerishlick, Gaelle Boncompain and Franck Perez for sharing plasmids and expertise for RUSH experiments. We thank Stefan Donat and Jan Schmoranzer of the AMBIO imaging center (Charité Berlin) for the technical assistance for spinning disk experiments and our lab manager Giorgia Carai for general technical assistance.

Author contribution

A.S., P.A. and F.B. conceived the project. A.S., P.A., V.N., A. H., A.K., S.H., C.R., C.S., A.G., J.M., D.P. and V.H. F.B. designed and performed experiments. A.S., P.A., V.N., A.H., A.K., S.H., A.G. and C.R. performed image analysis. A.S., P.A., V.N., A.H., A.K., S.H., C.R., C.S., E.Ö., P.L., A.G., E.F., J.M. generated plasmids and knock in/out cell lines. A.S., P.A. and F.B. wrote the manuscript with input from all authors.

Data availability

The data presented in this publication is available from the authors upon reasonable request.

References

1 Robinson, M. S. Forty Years of Clathrin-coated Vesicles. *Traffic* **16**, 1210-1238, doi:10.1111/tra.12335 (2015).

2 Ford, C., Parchure, A., von Blume, J. & Burd, C. G. Cargo sorting at the trans-Golgi network at a glance. *Journal of Cell Science* **134**, jcs259110, doi:10.1242/jcs.259110 (2021).

3 Traub, L. M., Ostrom, J. A. & Kornfeld, S. Biochemical dissection of AP-1 recruitment onto Golgi membranes. *Journal of Cell Biology* **123**, 561-573, doi:10.1083/jcb.123.3.561 (1993).

4 Ooi, C. E., Dell'Angelica, E. C. & Bonifacino, J. S. ADP-Ribosylation Factor 1 (ARF1) Regulates Recruitment of the AP-3 Adaptor Complex to Membranes. *Journal of Cell Biology* **142**, 391-402, doi:10.1083/jcb.142.2.391 (1998).

5 Ren, X., Farías, Ginny G., Canagarajah, Bertram J., Bonifacino, Juan S. & Hurley, James H. Structural Basis for Recruitment and Activation of the AP-1 Clathrin Adaptor Complex by Arf1. *Cell* **152**, 755-767, doi:10.1016/j.cell.2012.12.042 (2013).

6 Dell'Angelica, E. C., Klumperman, J., Stoorvogel, W. & Bonifacino, J. S. Association of the AP-3 Adaptor Complex with Clathrin. *Science* **280**, 431-434, doi:10.1126/science.280.5362.431 (1998).

7 Hirst, J. *et al.* A Family of Proteins with γ-Adaptin and Vhs Domains That Facilitate Trafficking between the Trans-Golgi Network and the Vacuole/Lysosome. *Journal of Cell Biology* **149**, 67-80, doi:10.1083/jcb.149.1.67 (2000).

8 Hirst, J., Irving, C. & Borner, G. H. H. Adaptor Protein Complexes AP-4 and AP-5: New Players in Endosomal Trafficking and Progressive Spastic Paraplegia. *Traffic* **14**, 153-164, doi:doi.org/10.1111/tra.12028 (2013).

9 Huang, Y. *et al.* Visualization of Protein Sorting at the Trans-Golgi Network and Endosomes Through Super-Resolution Imaging. *Frontiers in Cell and Developmental Biology* **7** (2019).

10 Solinger, J. A., Rashid, H.-O., Prescianotto-Baschong, C. & Spang, A. FERARI is required for Rab11-dependent endocytic recycling. *Nature Cell Biology* **22**, 213-224, doi:10.1038/s41556-019-0456-5 (2020).

11 Solinger, J. A., Rashid, H.-O. & Spang, A. FERARI and cargo adaptors coordinate cargo flow through sorting endosomes. *Nature Communications* **13**, 4620, doi:10.1038/s41467-022-32377-y (2022).

12 Wightman, R. M. & Haynes, C. L. Synaptic vesicles really do kiss and run. *Nature Neuroscience* **7**, 321-322, doi:10.1038/nn0404-321 (2004).

13 Solinger, J. A. & Spang, A. Sorting of cargo in the tubular endosomal network. *BioEssays* **44**, 2200158, doi:10.1002/bies.202200158 (2022).

14 Puertollano, R., Aguilar, R. C., Gorshkova, I., Crouch, R. J. & Bonifacino, J. S. Sorting of Mannose 6-Phosphate Receptors Mediated by the GGAs. *Science* **292**, 1712-1716, doi:10.1126/science.1060750 (2001).

15 Sönnichsen, B., De Renzis, S., Nielsen, E., Rietdorf, J. & Zerial, M. Distinct Membrane Domains on Endosomes in the Recycling Pathway Visualized by Multicolor Imaging of Rab4, Rab5, and Rab11. *Journal of Cell Biology* **149**, 901-914, doi:10.1083/jcb.149.4.901 (2000).

16 Trucco, A. *et al.* Secretory traffic triggers the formation of tubular continuities across Golgi sub-compartments. *Nature Cell Biology* **6**, 1071-1081, doi:10.1038/ncb1180 (2004).

17 Mesaki, K., Tanabe, K., Obayashi, M., Oe, N. & Takei, K. Fission of Tubular Endosomes Triggers Endosomal Acidification and Movement. *PLOS ONE* **6**, e19764, doi:10.1371/journal.pone.0019764 (2011).

18 Temkin, P. *et al.* SNX27 mediates retromer tubule entry and endosome-to-plasma membrane trafficking of signalling receptors. *Nature Cell Biology* **13**, 715-721, doi:10.1038/ncb2252 (2011).

19 Waguri, S. *et al.* Visualization of TGN to Endosome Trafficking through Fluorescently Labeled MPR and AP-1 in Living Cells. *Molecular Biology of the Cell* **14**, 142-155, doi:10.1091/mbc.e02-06-0338 (2002).
20 Bottanelli, F. *et al.* A novel physiological role for ARF1 in the formation of bidirectional tubules from the Golgi. *Molecular Biology of the Cell* **28**, 1676-1687, doi:10.1091/mbc.e16-12-0863 (2017).
21 Krauss, M. *et al.* Arf1-GTP-induced Tubule Formation Suggests a Function of Arf Family Proteins in Curvature Acquisition at Sites of Vesicle Budding *Journal of Biological Chemistry* **283**, 27717-27723, doi:10.1074/jbc.M804528200 (2008).
22 Stoorvogel, W., Oorschot, V. & Geuze, H. J. A novel class of clathrin-coated vesicles budding from endosomes. *Journal of Cell Biology* **132**, 21-33, doi:10.1083/jcb.132.1.21 (1996).
23 Peden, A. A. *et al.* Localization of the AP-3 adaptor complex defines a novel endosomal exit site for lysosomal membrane proteins. *Journal of Cell Biology* **164**, 1065-1076, doi:10.1083/jcb.200311064 (2004).
24 Raote, I. *et al.* TANGO1 membrane helices create a lipid diffusion barrier at curved membranes. *eLife* **9**, e57822, doi:10.7554/eLife.57822 (2020).
25 Weigel, A. V. *et al.* ER-to-Golgi protein delivery through an interwoven, tubular network extending from ER. *Cell* **184**, 2412-2429 (2021).
26 Shomron, O. *et al.* COPII collar defines the boundary between ER and ER exit site and does not coat cargo containers. *Journal of Cell Biology* **220**, e201907224, doi:10.1083/jcb.201907224 (2021).
27 Wong-Dilworth, L. *et al.* STED imaging of endogenously tagged ARF GTPases reveals their distinct nanoscale localizations. *Journal of Cell Biology* **222**, e202205107, doi:10.1083/jcb.202205107 (2023).
28 Gibson, T. J., Seiler, M. & Veitia, R. A. The transience of transient overexpression. *Nature Methods* **10**, 715-721, doi:10.1038/nmeth.2534 (2013).
29 Moriya, H. Quantitative nature of overexpression experiments. *Molecular Biology of the Cell* **26**, 3932-3939, doi:10.1091/mbc.E15-07-0512 (2015).
30 Stockhammer, A. & Bottanelli, F. Appreciating the small things in life: STED microscopy in living cells. *Journal of Physics D: Applied Physics* **54**, 033001, doi:10.1088/1361-6463/abac81 (2021).
31 Bottanelli, F. *et al.* Two-colour live-cell nanoscale imaging of intracellular targets. *Nature Communications* **7**, 10778, doi:10.1038/ncomms10778 (2016).
32 Xue, L., Karpenko, I. A., Hiblot, J. & Johnsson, K. Imaging and manipulating proteins in live cells through covalent labeling. *Nature Chemical Biology* **11**, 917-923, doi:10.1038/nchembio.1959 (2015).
33 Klumperman, J. & Raposo, G. The Complex Ultrastructure of the Endolysosomal System. *Cold Spring Harbor Perspectives in Biology* **6** (2014).
34 Carlton, J. *et al.* Sorting nexin-1 mediates tubular endosome-to-TGN transport through coincidence sensing of high-curvature membranes and 3-phosphoinositides. *Current biology* **14**, 1791-1800 (2004).
35 van Weering, J. R. T. & Cullen, P. J. Membrane-associated cargo recycling by tubule-based endosomal sorting. *Seminars in Cell & Developmental Biology* **31**, 40-47, doi:10.1016/j.semcdb.2014.03.015 (2014).
36 Boucrot, E., Saffarian, S., Zhang, R. & Kirchhausen, T. Roles of AP-2 in Clathrin-Mediated Endocytosis. *PLOS ONE* **5**, e10597, doi:10.1371/journal.pone.0010597 (2010).
37 Theos, A. C. *et al.* Functions of Adaptor Protein (AP)-3 and AP-1 in Tyrosinase Sorting from Endosomes to Melanosomes. *Molecular Biology of the Cell* **16**, 5356-5372, doi:10.1091/mbc.e05-07-0626 (2005).
38 Huang, F., Nesterov, A., Carter, R. E. & Sorkin, A. Trafficking of Yellow-Fluorescent-Protein-Tagged µ1 Subunit of Clathrin Adaptor AP-1 Complex in Living Cells. *Traffic* **2**, 345-357, doi:10.1034/j.1600-0854.2001.25020506.x (2001).

39 Hirst, J. *et al.* Distinct and overlapping roles for AP-1 and GGAs revealed by the "knocksideways" system. *Curr Biol* **22**, 1711-1716, doi:10.1016/j.cub.2012.07.012 (2012).
40 Murk, J. L. A. N. *et al.* Influence of aldehyde fixation on the morphology of endosomes and lysosomes: quantitative analysis and electron tomography. *Journal of Microscopy* **212**, 81-90, doi:10.1046/j.1365-2818.2003.01238.x (2003).
41 Boehm, M., Aguilar, R. C. & Bonifacino, J. S. Functional and physical interactions of the adaptor protein complex AP-4 with ADP-ribosylation factors (ARFs). *The EMBO Journal* **20**, 6265-6276, doi:10.1093/emboj/20.22.6265 (2001).
42 Gallusser, A. & Kirchhausen, T. The beta 1 and beta 2 subunits of the AP complexes are the clathrin coat assembly components. *The EMBO Journal* **12**, 5237-5244, doi:10.1002/j.1460-2075.1993.tb06219.x (1993).
43 Simpson, F., Peden, A. A., Christopoulou, L. & Robinson, M. S. Characterization of the Adaptor-related Protein Complex, AP-3. *Journal of Cell Biology* **137**, 835-845, doi:10.1083/jcb.137.4.835 (1997).
44 Faúndez, V., Horng, J.-T. & Kelly, R. B. A Function for the AP3 Coat Complex in Synaptic Vesicle Formation from Endosomes. *Cell* **93**, 423-432, doi:10.1016/S0092-8674(00)81170-8 (1998).
45 Peden, A. A., Rudge, R. E., Lui, W. W. Y. & Robinson, M. S. Assembly and function of AP-3 complexes in cells expressing mutant subunits. *Journal of Cell Biology* **156**, 327-336, doi:10.1083/jcb.200107140 (2002).
46 Kural, C. *et al.* Dynamics of intracellular clathrin/AP1-and clathrin/AP3-containing carriers. *Cell reports* **2**, 1111-1119 (2012).
47 Dell'Angelica, E. C. *et al.* Ggas: A Family of Adp Ribosylation Factor-Binding Proteins Related to Adaptors and Associated with the Golgi Complex. *Journal of Cell Biology* **149**, 81-94, doi:10.1083/jcb.149.1.81 (2000).
48 Miserey-Lenkei, S. *et al.* Rab and actomyosin-dependent fission of transport vesicles at the Golgi complex. *Nature Cell Biology* **12**, 645-654, doi:10.1038/ncb2067 (2010).
49 Boncompain, G. *et al.* Synchronization of secretory protein traffic in populations of cells. *Nature Methods* **9**, 493-498, doi:10.1038/nmeth.1928 (2012).
50 Sundberg, E. L., Deng, Y. & Burd, C. G. Monitoring Sphingolipid Trafficking in Cells using Fluorescence Microscopy. *Current Protocols in Cell Biology* **82**, e67, doi:doi.org/10.1002/cpcb.67 (2019).
51 Ang, A. L. *et al.* Recycling endosomes can serve as intermediates during transport from the Golgi to the plasma membrane of MDCK cells. *Journal of Cell Biology* **167**, 531-543, doi:10.1083/jcb.200408165 (2004).
52 Lock, J. G. & Stow, J. L. Rab11 in Recycling Endosomes Regulates the Sorting and Basolateral Transport of E-Cadherin. *Molecular Biology of the Cell* **16**, 1744-1755, doi:10.1091/mbc.e04-10-0867 (2005).
53 Hirst, J., Borner, G. H. H., Harbour, M. & Robinson, M. S. The Aftiphilin/p200/γ-Synergin Complex. *Molecular Biology of the Cell* **16**, 2554-2565, doi:10.1091/mbc.e04-12-1077 (2005).
54 Navarro Negredo, P., Edgar, J. R., Manna, P. T., Antrobus, R. & Robinson, M. S. The WDR11 complex facilitates the tethering of AP-1-derived vesicles. *Nature Communications* **9**, 596, doi:10.1038/s41467-018-02919-4 (2018).
55 Hooy, R. M., Iwamoto, Y., Tudorica, D. A., Ren, X. & Hurley, J. H. Self-assembly and structure of a clathrin-independent AP-1:Arf1 tubular membrane coat. *Science Advances* **8**, eadd3914, doi:10.1126/sciadv.add3914 (2022).
56 Salazar, G. *et al.* BLOC-1 Complex Deficiency Alters the Targeting of Adaptor Protein Complex-3 Cargoes. *Molecular Biology of the Cell* **17**, 4014-4026, doi:10.1091/mbc.e06-02-0103 (2006).
57 Casler, J. C., Papanikou, E., Barrero, J. J. & Glick, B. S. Maturation-driven transport and AP-1–dependent recycling of a secretory cargo in the Golgi. *Journal of Cell Biology* **218**, 1582-1601, doi:10.1083/jcb.201807195 (2019).

58 Kreitzer, G., Marmorstein, A., Okamoto, P., Vallee, R. & Rodriguez-Boulan, E. Kinesin and dynamin are required for post-Golgi transport of a plasma-membrane protein. *Nature Cell Biology* **2**, 125-127, doi:10.1038/35000081 (2000).
59 Jones, S. M., Howell, K. E., Henley, J. R., Cao, H. & McNiven, M. A. Role of dynamin in the formation of transport vesicles from the trans-Golgi network. *Science* **279**, 573-577 (1998).
60 Altschuler, Y. *et al.* Redundant and Distinct Functions for Dynamin-1 and Dynamin-2 Isoforms. *Journal of Cell Biology* **143**, 1871-1881, doi:10.1083/jcb.143.7.1871 (1998).
61 Kasai, K., Shin, H.-W., Shinotsuka, C., Murakami, K. & Nakayamat, K. Dynamin II Is Involved in Endocytosis but Not in the Formation of Transport Vesicles from the trans -Golgi Network11. *The Journal of Biochemistry* **125**, 780-789, doi:10.1093/oxfordjournals.jbchem.a022349 (1999).
62 Balla, A., Tuymetova, G., Barshishat, M., Geiszt, M. & Balla, T. Characterization of Type II Phosphatidylinositol 4-Kinase Isoforms Reveals Association of the Enzymes with Endosomal Vesicular Compartments *. *Journal of Biological Chemistry* **277**, 20041-20050, doi:10.1074/jbc.M111807200 (2002).
63 Doray, B., Ghosh, P., Griffith, J., Geuze Hans, J. & Kornfeld, S. Cooperation of GGAs and AP-1 in Packaging MPRs at the Trans-Golgi Network. *Science* **297**, 1700-1703, doi:10.1126/science.1075327 (2002).
64 Hirst, J., Motley, A., Harasaki, K., Peak Chew, S. Y. & Robinson, M. S. EpsinR: an ENTH Domain-containing Protein that Interacts with AP-1. *Molecular Biology of the Cell* **14**, 625-641, doi:10.1091/mbc.e02-09-0552 (2002).
65 Fujii, S. *et al.* Recycling endosomes attach to the trans-side of Golgi stacks in Drosophila and mammalian cells. *Journal of Cell Science* **133**, jcs236935, doi:10.1242/jcs.236935 (2020).
66 Perret, E., Lakkaraju, A., Deborde, S., Schreiner, R. & Rodriguez-Boulan, E. Evolving endosomes: how many varieties and why? *Current Opinion in Cell Biology* **17**, 423-434, doi:10.1016/j.ceb.2005.06.008 (2005).
67 Fölsch, H. Role of the epithelial cell-specific clathrin adaptor complex AP-1B in cell polarity. *Cellular Logistics* **5**, e1074331, doi:10.1080/21592799.2015.1074331 (2015).
68 Essletzbichler, P. *et al.* Megabase-scale deletion using CRISPR/Cas9 to generate a fully haploid human cell line. *Genome Research* **24**, 2059-2065 (2014).
69 Abramoff, M., Magalhães, P. & Ram, S. J. Image Processing with ImageJ. *Biophotonics International* **11**, 36-42 (2004).
70 Butkevich, A. N., Lukinavičius, G., D'Este, E. & Hell, S. W. Cell-Permeant Large Stokes Shift Dyes for Transfection-Free Multicolor Nanoscopy. *Journal of the American Chemical Society* **139**, 12378-12381, doi:10.1021/jacs.7b06412 (2017).
71 Luckner, M. & Wanner, G. Precise and economic FIB/SEM for CLEM: with 2 nm voxels through mitosis. *Histochemistry and Cell Biology* **150**, 149-170, doi:10.1007/s00418-018-1681-x (2018).
72 Lord, S. J., Velle, K. B., Mullins, R. D. & Fritz-Laylin, L. K. SuperPlots: Communicating reproducibility and variability in cell biology. *Journal of Cell Biology* **219**, e202001064, doi:10.1083/jcb.202001064 (2020).
73 Bolte, S. & CordeliÈRes, F. P. A guided tour into subcellular colocalization analysis in light microscopy. *Journal of Microscopy* **224**, 213-232, doi:10.1111/j.1365-2818.2006.01706.x (2006).
74 Grimm, J. B. *et al.* A General Method to Improve Fluorophores Using Deuterated Auxochromes. *JACS Au* **1**, 690-696, doi:10.1021/jacsau.1c00006 (2021).
75 Grimm, J. B. *et al.* A general method to optimize and functionalize red-shifted rhodamine dyes. *Nature Methods* **17**, 815-821, doi:10.1038/s41592-020-0909-6 (2020).